

# Learning Noise via Dynamical Decoupling of Entangled Qubits

Trevor McCourt,<sup>1,2</sup> Charles Neill,<sup>3</sup> Kenny Lee,<sup>3</sup> Chris Quintana,<sup>3</sup> Yu Chen,<sup>3</sup> Julian Kelly,<sup>3</sup> V. N. Smelyanskiy,<sup>3</sup> M. I. Dykman,<sup>4</sup> Alexander Korotkov,<sup>3</sup> Isaac L. Chuang,<sup>1,5</sup> and A. G. Petukhov<sup>3</sup>

<sup>1</sup>*Department of Electrical Engineering and Computer Science,  
Massachusetts Institute of Technology, Cambridge, MA 02139, USA*

<sup>2</sup>*Department of Physics, Co-Design Center for Quantum Advantage,  
Massachusetts Institute of Technology, Cambridge, Massachusetts 02139, USA*

<sup>3</sup>*Google Quantum AI, Santa Barbara, CA*

<sup>4</sup>*Department of Physics and Astronomy, Michigan State University, East Lansing, MI 48824, USA*

<sup>5</sup>*Department of Physics, Massachusetts Institute of Technology, Cambridge, MA 02139, USA*

(Dated: January 28, 2022)

Noise in entangled quantum systems is difficult to characterize due to many-body effects involving multiple degrees of freedom. This noise poses a challenge to quantum computing, where two-qubit gate performance is critical. Here, we develop and apply multi-qubit dynamical decoupling sequences that characterize noise that occurs during two-qubit gates. In our superconducting system comprised of Transmon qubits with tunable couplers, we observe noise that is consistent with flux fluctuations in the coupler that simultaneously affects both qubits and induces noise in their entangling parameter. The effect of this noise on the qubits is very different from the well-studied single-qubit dephasing. Additionally, steps are observed in the decoupled signals, implying the presence of non-Gaussian noise.

Producing interesting, large-scale, quantum dynamics in engineered systems is being made increasingly possible by the advancement of superconducting qubits. Transmon qubits that use frequency tunable couplers to realize inter-qubit interactions have been successful at this task in the areas of quantum simulation [1–3], quantum chemistry [4], and theoretical computer science [5–8]. Imperative to this is the ability to generate entanglement using high-fidelity two-qubit gates [9, 10]. As control of these gates is improved, their performance will start to become limited by system-environment interaction. The characterization and eventual mitigation of this noise producing interaction is therefore critical to continual forward progress.

Traditionally, low-frequency noise characterization in qubits has been dedicated to the study of single-qubit dephasing noise. This is modeled as either a qubit coupling to external quantum degrees of freedom or as classical stochastic fluctuations in the qubit frequency [11]. Most often, the noise is assumed to have Gaussian statistics. In this Gaussian scenario, sophisticated tools based on dynamical decoupling have been developed to characterize the power spectral density of the noise [12–14]. There have also been efforts to characterize noise outside of this regime. These have been focused on measuring the higher-order moments of single-qubit non-Gaussian dephasing [15, 16] as well as characterizing spatially correlated Gaussian dephasing noise [17–19].

Studies of single-qubit dephasing may be sufficient to understand the behavior of small systems involving only one or a few qubits. However, large systems have many degrees of freedom, and therefore many channels through which noise can enter. For example, noise that occurs

during two-qubit gates may lead to collective noise that affects two qubits simultaneously. Understanding these collective noise mechanisms in the context of quantum computing will be important for implementing NISQ algorithms in the near term and building a fault-tolerant quantum computer in the long term. The difficulty in characterizing noise in larger systems stems from the fact that measurement of a particular kind of noise may be confounded by competing error mechanisms, as larger systems are generally more difficult to control precisely than the small ones.

In this Letter, we characterize noise that occurs during two-qubit gates. The gate we study is performed using a tunable coupler that modulates the qubit-qubit coupling. Our key observation is that the primary source of noise is frequency fluctuations of this coupler. These fluctuations lead to noise in the entangling parameter  $g$ , the coupling strength between the two qubits. The noise is therefore turned on during a gate operation and affects two qubits simultaneously, in qualitative distinction from single-qubit dephasing. We show that this fundamentally two-qubit noise can be studied by driving pairs of qubits through two-qubit pulse sequences with interleaved coupler and qubit frequency control. We find that in many samples this noise is composed of Gaussian  $1/f$  noise, similar to the noise dominating single qubit dephasing, and a signal from a few random telegraph fluctuators with correlation times on the order of 100  $\mu$ s. These findings are significant because both the collective and non-Gaussian nature of the observed noise demand new error mitigation techniques. Additionally, the clean signatures of non-Gaussian noise that we see are a significant departure from what is typically assumed and observed in

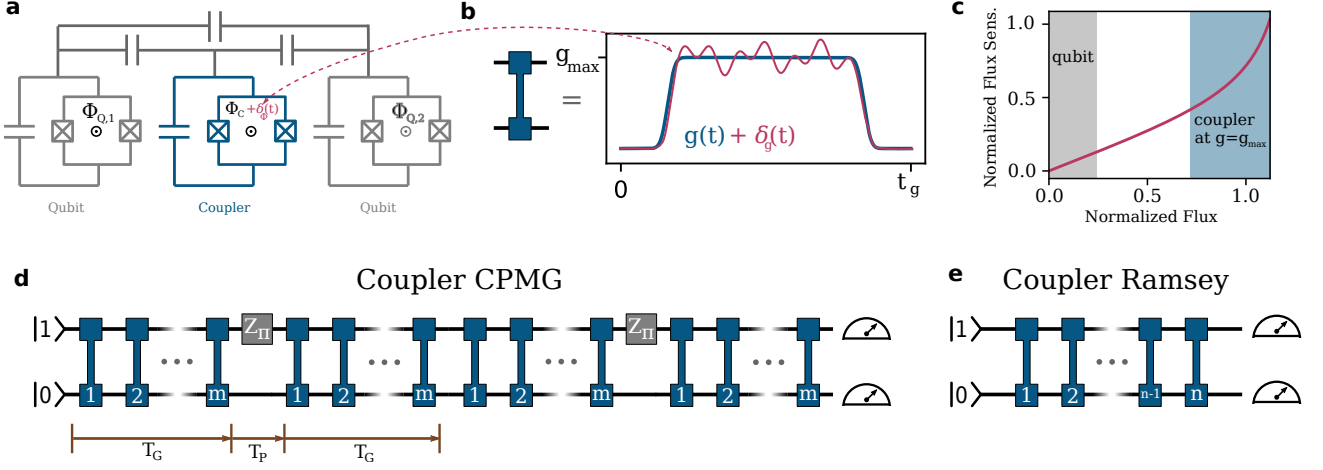


FIG. 1. **Circuits for entangled noise metrology** **a** Simplified circuit diagram for two qubits and the tunable coupler. The qubit frequencies  $\omega_j$  are modulated by changing  $\Phi_{Q,j}$ . The coupler frequency is changed significantly during two-qubit gates via  $\Phi_C$ . **b** Schematic of the time-dependent coupling  $g(t)$  enacted during two-qubit gates. The coupler flux noise  $\delta_\Phi(t)$  generates coupling fluctuations  $\delta_g(t)$  according to Eq. 4. **c** Flux sensitivity  $\chi$  (Eq. 5) vs external flux. The qubits are generally operated at frequencies with much lower flux sensitivity than the coupler. **d** Circuit diagram showing the Coupler CPMG sequence. Shown here are  $n = 2$  repetitions of a pulse sequence involving  $2m$  two-qubit gates that are separated by a qubit frequency  $\pi$  pulse. The two-qubit gates serve to expose the qubits to  $g$ -noise, which is refocused by the frequency pulse. The decay of the pseudo-qubit  $\langle \sigma_z \rangle$  observable is measured at the end of the circuit, which can be used to characterize the noise. See supplementary material section J for further examples. **e** Circuit diagram showing the Coupler Ramsey sequence involving  $n$  two-qubit gates, which can be used to measure the response of the qubits to  $g$ -noise in the absence of refocusing pulses.

condensed matter systems, where Gaussian  $1/f$  noise is ubiquitous [20–23].

We begin by introducing the theory of flux noise entering through the coupler and a technique for measuring it. We then present the measurement results and show that while they match well what would be expected for coupler flux noise, they do not agree well with Gaussian theory. Finally, we generalize to a non-Gaussian model of the noise and validate it with further experiments.

The single excitation subspace of two qubits is spanned by the states  $|01\rangle$  and  $|10\rangle$  and forms a pseudo-qubit with the Hamiltonian

$$H = \frac{1}{2} (\omega(t) + \delta\omega(t)) \sigma_z + (g(t) + \delta g(t)) \sigma_x, \quad (1)$$

where  $\sigma_z = |01\rangle\langle 01| - |10\rangle\langle 10|$  and  $\sigma_x = |01\rangle\langle 10| + |10\rangle\langle 01|$ . Here  $\omega(t)$  and  $\delta\omega(t)$  are the control and noise contributions to the difference of the qubit frequencies, respectively, while  $g(t)$  and  $\delta g(t)$  are the control and noise contributions to the inter-qubit coupling.

During two-qubit gates the two qubits are on resonance,  $\omega(t) = 0$ . In this case,  $\delta\omega(t)$  and  $g(t) + \delta g(t)$  can be considered respectively as  $z$  and  $x$  components of an effective magnetic field. The Bloch vector of our effective two-level system undergoes Larmor precession around the instantaneous axis, which is almost parallel to the  $x$ -field, with the instantaneous Larmor frequency given by

$$\omega_L(t) \simeq 2g(t) + 2\delta g(t) + \frac{\delta\omega^2(t)}{4g(t)}. \quad (2)$$

From this, we can see that coupler noise will dominate during two-qubit gates:  $\delta g(t)$  shows up to first order in the dynamics while  $\delta\omega(t)$  only shows up to second-order and is suppressed by a factor of  $g(t)$ .

Coupler noise physically results from coupler frequency fluctuations. In our tunable coupler system depicted in Fig. 1, the qubit frequencies  $\omega_q$  and the coupler frequencies  $\omega_c$  are controllable via the external fluxes,  $\Phi_q$  and  $\Phi_c$ , respectively and the relation between  $\omega$  and  $\Phi$  is  $\omega \simeq \omega_{\max} \sqrt{\left| \cos\left(\frac{\pi\Phi}{\Phi_0}\right) \right|}$ , where  $\Phi_0$  is the flux quantum. The coupling  $g$  developed between two qubits that are on resonance at  $\omega_q$  is given by [24]

$$g \simeq \left( k_d - k^2 \frac{\omega_q^2}{\omega_c^2 - \omega_q^2} \right) \frac{\omega_q}{2}, \quad (3)$$

where  $k$  and  $k_d$  are the indirect and direct coupling efficiencies that are functions of circuit parameters (see supplementary material section C). The pseudo-qubit defined in Eq. 1 is therefore completely controllable via low-frequency manipulation of the qubit and coupler flux biases and no microwave control is necessary to implement dynamical decoupling of the entangled qubits. Another characteristic feature of our method is the ability to post-select experimental outcomes belonging only to the pseudo-qubit subspace and separate the processes of collective dephasing from those of energy relaxation.

Fluctuations in  $\Phi$  lead to fluctuations in frequency, i.e. to flux noise, which is ubiquitous in SQUIDs [25]. During

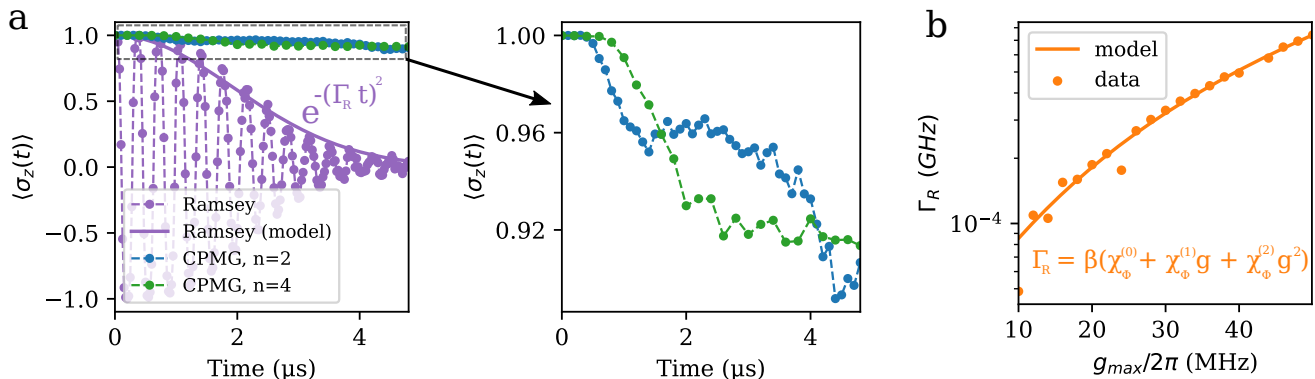


FIG. 2. **Experimentally observed Ramsey and CPMG dynamics.** **a** Comparing Coupler Ramsey decay of normalized population difference (Eq. 8) with  $g_{\text{max}} = 30\text{MHz}$  to decay under  $n = 2$  and  $n = 4$  Coupler CPMG sequences. The x-axis is total evolution time,  $t = nt_g$  for Ramsey and  $t = 2mnt_g$  for CPMG. The duration of a fixed  $n$  CPMG sequence is modified by changing  $m$ . We see that the CPMG sequences effectively mitigate most of the decoherence, suggesting that most of the noise power is at low frequencies. The Gaussian shape of the Ramsey decay envelope is typical of  $1/f$ -type noise (see Eq. 6). When observed in detail, the CPMG decay envelopes display behavior not predicted by Gaussian theory. Increasing the number of CPMG pulses does not increase noise protection as predicted by Eq. 7; the curves braid and have steps. All data points are the average of 10000 samples. **b** Ramsey decay rate  $\Gamma_R$  vs  $g_{\text{max}}$ . We see that the decay rate is strongly dependent on  $g_{\text{max}}$ , crossing an order of magnitude in 30 MHz. The  $g_{\text{max}}$ -dependence is well-predicted by Eq. 4 given typical circuit parameters.

gates, the sensitivity of the coupler frequency to flux noise is substantially larger than that of the qubit, see Fig. 1 b. Noise in the coupler frequency leads to fluctuations in  $g$ . The fluctuation  $\delta g(t)$  in the Hamiltonian (1) can be expressed through coupler flux fluctuations  $\delta\Phi_c(t)$  as follows

$$\delta g(t) = 2\pi\tilde{\chi}_\Phi(g)\delta\Phi_c(t) = \lambda(g)\xi(t), \quad (4)$$

where the flux sensitivity of  $g$  is defined as

$$\tilde{\chi}_\Phi = \frac{1}{2\pi} \left| \frac{dg}{d\Phi_c} \right| \simeq \chi_\Phi^{(0)} + \chi_\Phi^{(1)}g + \chi_\Phi^{(2)}g^2. \quad (5)$$

Here  $\xi(t)$  is a dimensionless classical random variable modeling flux fluctuations with characteristic amplitude  $\delta\Phi_m$ , and  $\lambda(g) = 2\pi\tilde{\chi}_\Phi(g)\delta\Phi_m$  is the amplitude of  $g$ -noise. It can be shown (see supplementary material section C) that in the studied parameter range the quadratic dependence of  $\tilde{\chi}_\Phi(g)$ , displayed in Eq. 5, follows directly from Eq. 3.

The effect of  $g$ -noise on the pseudo-qubit defined in Eq. 1 may be characterized using what we call the Coupler CPMG pulse sequence. In this sequence, the pseudo-qubit is initialized in the state  $|01\rangle$  via a microwave pulse. It is then exposed to  $n$  repetitions of a spin echo-like pulse sequence [26], each of which consists of a fast  $\pi$ -rotation around  $z$ -axis ( $\sigma_z$   $\pi$ -pulse) buffered before and after by exposure to  $g$ -noise for time  $T_G$ . The  $\sigma_z$  pulse has the effect of refocusing the  $\sigma_x$   $g$ -noise. This exposure to  $g$ -noise is accomplished by  $m$  repetitions of a Floquet-calibrated [1] two-qubit gate with duration  $t_g$  for which  $\omega = 0$  and  $|g| > 0$ , see Fig. 1 b. There are a total of  $2m$  two-qubit gates between refocusing pulses; the total time between refocusing pulses is therefore  $2mt_g$ . After

the  $n$  echo sequences are completed, we can measure the pseudo-qubit observable  $\langle \sigma_z \rangle$ , which will decay due to  $g$ -noise. Studying the decay of this observable will reveal the character of the noise. The Coupler CPMG pulse sequence is shown in Fig. 1 d. This pulse sequence is analogous to standard, single qubit CPMG [27, 28], with the main difference being that it takes place in the  $z$ -y plane of the Bloch sphere instead of the  $x$ -y plane, so the direction of refocusing pulses and measurements must be adjusted accordingly. It is also desirable to observe the  $\sigma_z$  decay due to  $g$ -noise in the absence of the refocusing pulses. This may be done using the Coupler Ramsey pulse sequence, see Fig. 1 e.

The statistics of  $\xi(t)$  dictate what type of decay we expect to see during these sequences. A common assumption is  $\xi(t)$  is a Gaussian random process, which means that  $\xi(t)$  has a jointly Gaussian distribution at all times. In the typical case where  $\xi(t)$  is Gaussian  $1/f$  noise, for decay under the Coupler Ramsey sequence we would expect (up to logarithmic corrections, see supplementary material section F),

$$\langle \sigma_z(t) \rangle \simeq e^{-(\Gamma_R t)^2} \cos(Gt), \quad \Gamma_R \propto \lambda, \quad (6)$$

where  $G$  is the coherent swap frequency. In the case of decay under an  $n$ -pulse CPMG sequence,

$$\langle \sigma_z(t) \rangle \simeq e^{-(\Gamma_C t)^2}, \quad \Gamma_C \propto \frac{\lambda}{\sqrt{n}}. \quad (7)$$

We experimentally characterize  $g$ -noise on our superconducting qubit device [7] by executing these sequences. We measure the observable

$$\frac{\langle \sigma_z \rangle}{\langle I \rangle} = \frac{\langle 01 | \rho(t) | 01 \rangle - \langle 10 | \rho(t) | 10 \rangle}{\langle 01 | \rho(t) | 01 \rangle + \langle 10 | \rho(t) | 10 \rangle}, \quad (8)$$

as a function of time, number of CPMG cycles, and maximum coupling  $g_{\max}$ . This normalization of  $\langle\sigma_z\rangle$  eliminates the effect of  $T_1$  noise in relevant cases, see supplementary material section E. We can compare the shapes of the measured decay envelopes with Eqs. 6 and 7, and the  $g$ -dependence of decay rates with Eq. 4 to test the theory that our device is susceptible to Gaussian noise entering through the flux bias during two-qubit gates.

As can be seen in Fig. 2 a, the experimentally measured Ramsey decay envelopes are well predicted by Gaussian  $1/f$  noise. Additionally, as shown in Fig. 2 b, the scaling of the Gaussian decay rate with  $g_{\max}$  agrees with the form of Eq. 4. Notably, the decay rate increases by an order of magnitude as  $g_{\max}$  is increased from 10 to 50 MHz, suggesting that this coupler noise heavily exceeds single qubit dephasing as an error mechanism during gates with large coupling, as predicted by Eq. 2. Additionally, the flux sensitivity function extracted matches the theory well. From the data we extract a value of  $\chi_{\Phi}^{(2)}/\chi_{\Phi}^{(1)} \approx 0.078$  ns, while a purely theoretical calculation using typical circuit parameters yields  $\chi_{\Phi}^{(2)}/\chi_{\Phi}^{(1)} \approx 0.08$  ns. This excellent agreement with theory strongly suggests that noise during two-qubit gates is dominated by flux noise in the coupler, as hypothesized.

The CPMG envelopes decay significantly slower than the Ramsey envelopes as would be predicted by Gaussian theory. However, as shown in Fig. 2 the details of these curves deviate significantly from what would be predicted by Gaussian  $1/f$  noise. While Eq. 7 predicts smooth decay, we see very clear steps in the decay curves. Additionally, the model predicts that the decay rate  $\Gamma_C$  should decrease proportionately to  $\frac{1}{\sqrt{n}}$ . This is not seen at all: the two curves "braid" and decay at the same rate.

The steps in the CPMG curves are difficult for any Gaussian noise model to produce (see supplementary material section G for further discussion on this). Therefore, these steps are signatures of non-Gaussian noise in our system.

It is reasonable to suggest that this non-Gaussian noise is the result of a small number of strongly coupled random telegraph noise (RTN) fluctuators, since Gaussian  $1/f$  noise may be produced via a superposition of a large number of weakly coupled fluctuators [29] (see supplementary material section B). The CPMG decay curve associated with single RTN fluctuator with correlation time  $t_c = \frac{1}{\gamma}$  is [30–32], see supplementary material section D,

$$\langle\sigma_z(t = 2mnt_g)\rangle = \begin{cases} e^{-2mn\gamma t_g} \left( q \frac{\cosh(n\alpha)}{\cosh(\alpha)} + \sinh(n\alpha) \right), & n \text{ odd} \\ e^{-2mn\gamma t_g} \left( q \frac{\sinh(n\alpha)}{\cosh(\alpha)} + \cosh(n\alpha) \right), & n \text{ even} \end{cases} \quad (9)$$

where

$$q = -\frac{4\lambda^2}{\Omega^2} + \frac{\gamma^2 \cosh(2m\Omega t_g)}{\Omega^2}, \quad (10)$$

$$\sinh(\alpha) = \frac{\gamma}{\Omega} \sinh(2m\Omega t_g),$$

and  $\Omega = \sqrt{\gamma^2 - 4\lambda^2}$  is the associated Rabi frequency.  $\lambda$  is taken to be the average value of  $\lambda(g(t))$  over a gate,

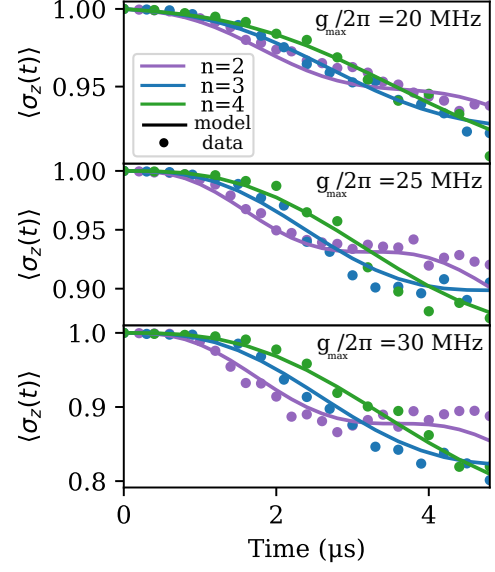


**FIG. 3. Braiding in the CPMG decay envelopes** Fitting a single-fluctuator model to CPMG decay envelopes (Eq. 9) for different values of  $n$  and  $g_{\max}$ . Each set of 3 curves is fit using only 2 parameters,  $\gamma$  and  $\lambda$ . Good agreement is found between theory and experiment. Fits for more values of  $n$  can be found in supplementary material section H. Typical values of  $t_c = \frac{1}{\gamma} \approx 50\mu\text{s}$ ,  $\frac{\lambda}{2\pi} \approx 0.1 - 1\text{MHz}$  (value depends strongly on  $g$ , see Fig. 4), and  $\Gamma_{\phi}^{-1} \approx 100\mu\text{s}$ . All data points are the average of 10000 samples.

see supplementary material section E for justification. It has also been assumed that  $T_P \ll T_C$  (as in Fig. 1 d), such that the CPMG cycle time is  $T_C = 2mt_g$ . The form of the solution depends heavily on  $\Omega$ . If  $\Omega$  is real, the solution is over-damped, and decays smoothly. If  $\Omega$  is imaginary, the solution is under-damped and has oscillatory components.

We can validate this model by repeating the previous CPMG measurements for more values of  $n$  and attempting to fit the data simultaneously. The results of this are shown in Fig. 3. The decay envelopes are excellently described by a single, under-damped RTN fluctuator alongside single qubit white noise dephasing, which adds a simple exponential prefactor  $e^{-\frac{\Gamma_{\phi}}{4}t}$  to Eq. 9, see supplementary material section E.

In each case, the fit fluctuator is strongly in the under-damped regime,  $2\lambda > \gamma$ . In this regime, as shown in supplementary material section I, Eq. 9 is well approximated by,

$$\langle\sigma_z(t = 2mnt_g)\rangle \approx e^{-2mnt_g\gamma} e^{n\epsilon \sin(2mt_g\omega)}, \quad (11)$$

where  $\Omega = i\bar{\omega}$  and  $\epsilon = \frac{\gamma}{\bar{\omega}}$ . For the data shown in Fig. 3 a,  $\epsilon \approx \frac{1}{100}$ . If the number of CPMG cycles is also modest,  $n\epsilon \ll 1$ , and this further reduces to,

$$\langle\sigma_z(t = 2mnt_g)\rangle \approx e^{-2mnt_g\gamma} \left( 1 + n\frac{\gamma}{\bar{\omega}} \sin(2mt_g\bar{\omega}) \right). \quad (12)$$



In this form, the dynamics are much more clear. The decay envelope will generally follow exponential decay and will produce steps with frequency  $\frac{\omega}{n}$ . The implication of this is that it is difficult to dynamically suppress the decoherence caused by this kind of noise: more than  $\frac{1}{\epsilon}$  echo pulses are required in time  $t$  to cause the trajectory to deviate significantly from exponential decay. This is significantly different than what would be expected for Gaussian  $1/f$  noise for example, for which protection increases monotonically and smoothly with  $n$ .

The scaling of the coupling strength of this single fluctuator with  $g$  can be established by taking CPMG data on the same pair of qubits over a range of values of  $g_{\max}$ . Fig. 4 shows the results of such an experiment.

The data can be fit well with a model that includes one slow, strongly coupled fluctuator, white flux noise (emulated by a fast fluctuator), and single-qubit dephasing. The inclusion of white flux noise was critical to achieving a good fit, which is physically reasonable, as echo sequences do not suppress this kind of noise at all. The slow fluctuator has a correlation time of approximately  $70\mu s$ . This is the strongly coupled, underdamped fluctuator that creates the steps seen in the data and the fit. The single-qubit dephasing rate represents white noise that does not scale with  $g$ , and the extracted value of  $\frac{1}{\Gamma_{\phi}} \approx 90\mu s$  is reasonable for this device. Ratio  $\chi_{\Phi}^{(2)}/\chi_{\Phi}^{(1)} \approx 0.12$  ns for this data, which is also within expectation.

It should be noted that this work alone is not enough to understand the physical origins of this non-Gaussian contribution to the noise. To do that, further study into the spatial dependence of the noise would have to be completed. Although this noise has been observed on several qubits in our system, this has not been studied systematically enough to determine if different qubits see fluctuators with similar parameters. Additionally, it would be impossible to tell if multiple pairs of qubits are seeing the same physical defect or just similar, independent defects with this kind of time-averaged, two-qubit measurement. These two situations may be discernible using time-averaged measurements taken after periodic pulse sequences on more than two qubits. This spatial dependence will be the subject of future study.

While the majority of this work was focused on the details of applying our technique to tunable-coupler Transmons, the basic methods transfer readily to other qubit architectures. As an example from trapped ion quantum computing, a similar technique could be used in the characterization of the effect of noise [33] on the coupling developed between ion electronic states during Mølmer-Sørensen gates [34].

This work has elucidated the importance of studying noise via the physics of a specific device, especially as larger and larger quantum computers are built. Indeed,

this approach is what allowed us to discover the dominant source of low-frequency noise that occurs during our two-qubit gates. Additionally, we have found very clear signatures of non-Gaussian, non  $1/f$  noise in our solid-

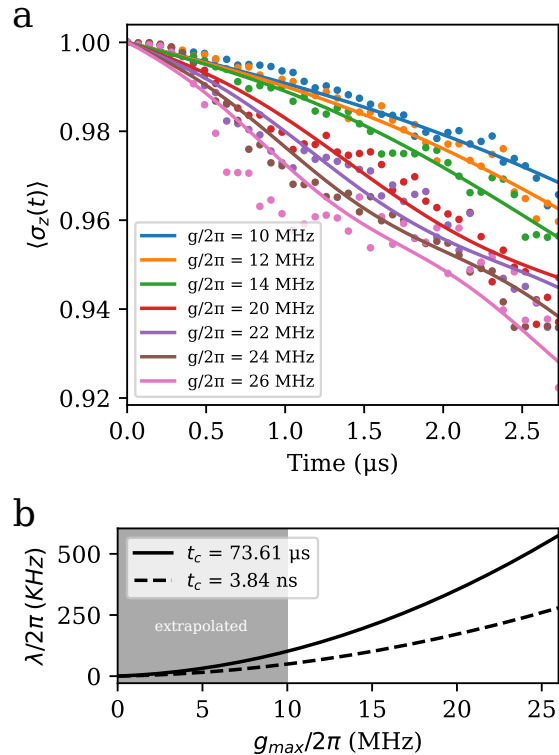


FIG. 4. **Extracting the scaling of telegraph noise amplitude.** **a**) Experimental data (dots) vs fit model (lines) for  $n = 1$  CPMG sequences at various values of  $g_{\max}$ . The fit value of  $T_{\phi}$  is approximately  $90\mu s$ , which is a reasonable result for this device. **b**) The extracted noise amplitude  $\lambda(g)$  for the two fluctuators. Note that the same function  $\chi_{\Phi}$  was used for both fluctuators; the  $g$ -noise amplitudes were only allowed to differ by an overall scale.

state device, which is quite atypical in the field. Further study of this kind of noise may reveal its physical origins, and yield insight into better design, fabrication or control of quantum devices.

## ACKNOWLEDGMENTS

TM was supported in part by the U.S. Department of Energy, Office of Science, National Quantum Information Science Research Centers, Co-Design Center for Quantum Advantage under contract DE-SC0012704. TM would like to thank John Chiaverini and John Martyn for their comments on the manuscript.

[1] C. Neill, T. McCourt, X. Mi, Z. Jiang, M. Y. Niu, W. Mruzckiewicz, I. Aleiner, F. Arute, K. Arya, J. Ata-

laya, and et al., *Nature* **594**, 508–512 (2021).

- [2] F. Arute, K. Arya, R. Babbush, D. Bacon, J. C. Bardin, R. Barends, A. Bengtsson, S. Boixo, M. Broughton, B. B. Buckley, D. A. Buell, B. Burkett, N. Bushnell, Y. Chen, Z. Chen, Y.-A. Chen, B. Chiaro, R. Collins, S. J. Cotton, W. Courtney, S. Demura, A. Derk, A. Dunsworth, D. Eppens, T. Eickl, C. Erickson, E. Farhi, A. Fowler, B. Foxen, C. Gidney, M. Giustina, R. Graff, J. A. Gross, S. Habegger, M. P. Harrigan, A. Ho, S. Hong, T. Huang, W. Huggins, L. B. Ioffe, S. V. Isakov, E. Jeffrey, Z. Jiang, C. Jones, D. Kafri, K. Kechedzhi, J. Kelly, S. Kim, P. V. Klimov, A. N. Korotkov, F. Kostritsa, D. Landhuis, P. Laptev, M. Lindmark, E. Lucero, M. Marthaler, O. Martin, J. M. Martinis, A. Marusczyk, S. McArdle, J. R. McClean, T. McCourt, M. McEwen, A. Megrant, C. Mejuto-Zaera, X. Mi, M. Mohseni, W. Mruczkiewicz, J. Mutus, O. Naaman, M. Neeley, C. Neill, H. Neven, M. Newman, M. Y. Niu, T. E. O'Brien, E. Ostby, B. Pató, A. Petukhov, H. Putterman, C. Quintana, J.-M. Reiner, P. Roushan, N. C. Rubin, D. Sank, K. J. Satzinger, V. Smelyanskiy, D. Strain, K. J. Sung, P. Schmitteckert, M. Szalay, N. M. Tubman, A. Vainsencher, T. White, N. Vogt, Z. J. Yao, P. Yeh, A. Zalcman, and S. Zanker, "Observation of separated dynamics of charge and spin in the fermi-hubbard model," (2020), [arXiv:2010.07965](https://arxiv.org/abs/2010.07965) [quant-ph].
- [3] A. T. K. Tan, S.-N. Sun, R. N. Tazhigulov, G. K.-L. Chan, and A. J. Minnich, "Realizing symmetry-protected topological phases in a spin-1/2 chain with next-nearest neighbor hopping on superconducting qubits," (2021), [arXiv:2112.10333](https://arxiv.org/abs/2112.10333) [quant-ph].
- [4] F. Arute, K. Arya, R. Babbush, D. Bacon, J. C. Bardin, R. Barends, S. Boixo, M. Broughton, B. B. Buckley, and et al., *Science* **369**, 1084–1089 (2020).
- [5] J. Kelly, R. Barends, A. G. Fowler, A. Megrant, E. Jeffrey, T. C. White, D. Sank, J. Y. Mutus, B. Campbell, Y. Chen, and et al., *Nature* **519**, 66–69 (2015).
- [6] Z. Chen, K. J. Satzinger, J. Atalaya, A. N. Korotkov, A. Dunsworth, D. Sank, C. Quintana, M. McEwen, R. Barends, P. V. Klimov, S. Hong, C. Jones, A. Petukhov, D. Kafri, S. Demura, B. Burkett, C. Gidney, A. G. Fowler, H. Putterman, I. Aleiner, F. Arute, K. Arya, R. Babbush, J. C. Bardin, A. Bengtsson, A. Bourassa, M. Broughton, B. B. Buckley, D. A. Buell, N. Bushnell, B. Chiaro, R. Collins, W. Courtney, A. R. Derk, D. Eppens, C. Erickson, E. Farhi, B. Foxen, M. Giustina, J. A. Gross, M. P. Harrigan, S. D. Harrington, J. Hilton, A. Ho, T. Huang, W. J. Huggins, L. B. Ioffe, S. V. Isakov, E. Jeffrey, Z. Jiang, K. Kechedzhi, S. Kim, F. Kostritsa, D. Landhuis, P. Laptev, E. Lucero, O. Martin, J. R. McClean, T. McCourt, X. Mi, K. C. Miao, M. Mohseni, W. Mruczkiewicz, J. Mutus, O. Naaman, M. Neeley, C. Neill, M. Newman, M. Y. Niu, T. E. O'Brien, A. Opremcak, E. Ostby, B. Pató, N. Redd, P. Roushan, N. C. Rubin, V. Shvarts, D. Strain, M. Szalay, M. D. Trevithick, B. Villalonga, T. White, Z. J. Yao, P. Yeh, A. Zalcman, H. Neven, S. Boixo, V. Smelyanskiy, Y. Chen, A. Megrant, and J. Kelly, "Exponential suppression of bit or phase flip errors with repetitive error correction," (2021), [arXiv:2102.06132](https://arxiv.org/abs/2102.06132) [quant-ph].
- [7] F. Arute *et al.*, *Nature* **574**, 505 (2019).
- [8] H.-Y. Huang, M. Broughton, J. Cotler, S. Chen, J. Li, M. Mohseni, H. Neven, R. Babbush, R. Kueng, J. Preskill, and J. R. McClean, "Quantum advantage in learning from experiments," (2021), [arXiv:2112.00778](https://arxiv.org/abs/2112.00778) [quant-ph].
- [9] Y. Sung, L. Ding, J. Braumüller, A. Vepsäläinen, B. Kannan, M. Kjaergaard, A. Greene, G. O. Samach, C. McNally, D. Kim, A. Melville, B. M. Niedzielski, M. E. Schwartz, J. L. Yoder, T. P. Orlando, S. Gustavsson, and W. D. Oliver, *Phys. Rev. X* **11**, 021058 (2021).
- [10] B. Foxen, C. Neill, A. Dunsworth, P. Roushan, B. Chiaro, A. Megrant, J. Kelly, Z. Chen, K. Satzinger, R. Barends, and et al., *Physical Review Letters* **125** (2020), [10.1103/physrevlett.125.120504](https://arxiv.org/abs/10.1103/physrevlett.125.120504).
- [11] G. S. Uhrig, *New Journal of Physics* **10** (2008), [10.1088/1367-2630/10/8/083024](https://arxiv.org/abs/10.1088/1367-2630/10/8/083024), [arXiv:0803.1427](https://arxiv.org/abs/0803.1427).
- [12] Ł. Cywiński, R. M. Lutchyn, C. P. Nave, and S. Das Sarma, *Physical Review B - Condensed Matter and Materials Physics* **77**, 1 (2008), [arXiv:0712.2225](https://arxiv.org/abs/0712.2225).
- [13] J. Bylander, S. Gustavsson, F. Yan, F. Yoshihara, K. Harrabi, G. Fitch, D. G. Cory, Y. Nakamura, J. S. Tsai, and W. D. Oliver, *Nature Physics* **7**, 565 (2011).
- [14] M. J. Biercuk, A. C. Doherty, and H. Uys, *Journal of Physics B: Atomic, Molecular and Optical Physics* **44** (2011), [10.1088/0953-4075/44/15/154002](https://arxiv.org/abs/10.1088/0953-4075/44/15/154002), [arXiv:1012.4262](https://arxiv.org/abs/1012.4262).
- [15] L. M. Norris, G. A. Paz-Silva, and L. Viola, *Physical Review Letters* **116**, 1 (2016), [arXiv:1512.01575](https://arxiv.org/abs/1512.01575).
- [16] Y. Sung, F. Beaudoin, L. M. Norris, F. Yan, D. K. Kim, J. Y. Qiu, U. von Lüpke, J. L. Yoder, T. P. Orlando, S. Gustavsson, L. Viola, and W. D. Oliver, *Nature Communications* **10**, 1 (2019), [arXiv:1903.01043](https://arxiv.org/abs/1903.01043).
- [17] G. A. Paz-Silva, L. M. Norris, and L. Viola, *Physical Review A* **95** (2017), [10.1103/physreva.95.022121](https://arxiv.org/abs/10.1103/physreva.95.022121).
- [18] P. Szankowski, M. Trippenbach, and L. Cywinski, *Physical Review A* **94** (2016), [10.1103/physreva.94.012109](https://arxiv.org/abs/10.1103/physreva.94.012109).
- [19] J. Krzywda, P. Szankowski, and L. Cywinski, *New Journal of Physics* **21** (2019), [10.1088/1367-2630/ab0ce7](https://arxiv.org/abs/10.1088/1367-2630/ab0ce7).
- [20] P. Dutta and P. M. Horn, *Rev. Mod. Phys.* **53**, 497 (1981).
- [21] R. J. Schoelkopf, P. Wahlgren, A. A. Kozhevnikov, P. Delsing, and D. E. Prober, *Science* **280**, 1238 (1998).
- [22] D. An, C. Matthiesen, E. Urban, and H. Häffner, *Physical Review A* **100** (2019), [10.1103/PhysRevA.100.063405](https://arxiv.org/abs/10.1103/PhysRevA.100.063405), [arXiv:1906.06489](https://arxiv.org/abs/1906.06489).
- [23] F. Yoshihara, Y. Nakamura, F. Yan, S. Gustavsson, J. Bylander, W. D. Oliver, and J.-S. Tsai, *Physical Review B* **89** (2014), [10.1103/physrevb.89.020503](https://arxiv.org/abs/10.1103/physrevb.89.020503).
- [24] F. Yan, P. Krantz, Y. Sung, M. Kjaergaard, D. L. Campbell, T. P. Orlando, S. Gustavsson, and W. D. Oliver, *Physical Review Applied* **10** (2018), [10.1103/PhysRevApplied.10.054062](https://arxiv.org/abs/10.1103/PhysRevApplied.10.054062), [arXiv:1803.09813](https://arxiv.org/abs/1803.09813).
- [25] R. Koch, J. Clarke, W. Goubau, J. Martinis, C. Pegrum, and D. van Harlingen, *Journal of Low Temperature Physics* **51**, 207 (1983).
- [26] E. L. Hahn, *Phys. Rev.* **80**, 580 (1950).
- [27] H. Y. Carr and E. M. Purcell, *Phys. Rev.* **94**, 630 (1954).
- [28] S. Meiboom and D. Gill, *Review of Scientific Instruments* **29**, 688 (1958), <https://doi.org/10.1063/1.1716296>.
- [29] F. Hooge, *IEEE Transactions on Electron Devices* **41**, 1926 (1994).
- [30] G. Ramon, *Physical Review B - Condensed Matter and Materials Physics* **92**, 1 (2015).
- [31] Y. M. Galperin, B. L. Altshuler, J. Bergli, and D. V. Shantsev, *Physical Review Letters* **96**, 1 (2006), [arXiv:0511238](https://arxiv.org/abs/0511238) [cond-mat].
- [32] L. Faoro and L. Viola, *Physical Review Letters* **92**, 1 (2004), [arXiv:0312159](https://arxiv.org/abs/0312159) [quant-ph].

- [33] D. Hayes, S. M. Clark, S. Debnath, D. Hucul, I. V. Inlek, K. W. Lee, Q. Quraishi, and C. Monroe, *Phys. Rev. Lett.* **109**, 020503 (2012).
- [34] K. Mølmer and A. Sørensen, *Physical Review Letters* **82**, 1835–1838 (1999).
- [35] V. I. Klyatskin, *Lectures on Dynamics of Stochastic Systems* (Elsevier, Amsterdam, 2011).
- [36] J. Bylander, S. Gustavsson, F. Yan, F. Yoshihara, K. Harrabi, G. Fitch, D. G. Cory, Y. Nakamura, J.-S. Tsai, and W. D. Oliver, *Nature Physics* **7**, 565–570 (2011).
- [37] D. H. Slichter, R. Vijay, S. J. Weber, S. Boutin, M. Boissonneault, J. M. Gambetta, A. Blais, and I. Siddiqi, *Physical Review Letters* **109** (2012), 10.1103/physrevlett.109.153601.
- [38] F. Yan, S. Gustavsson, J. Bylander, X. Jin, F. Yoshihara, D. G. Cory, Y. Nakamura, T. P. Orlando, and W. D. Oliver, *Nature communications* **4**, 2337 (2013).
- [39] F. Yoshihara, Y. Nakamura, F. Yan, S. Gustavsson, J. Bylander, W. D. Oliver, and J.-S. Tsai, *Physical Review B* **89** (2014), 10.1103/physrevb.89.020503.

# Appendices

## Table of Contents

---

Appendix A	Telegraph Noise	S1
Appendix B	1/f Noise From Telegraph Fluctuators	S2
Appendix C	Flux Sensitivity in Tunable Coupler Systems	S2
Appendix D	Direct averaging over Noise Trajectories	S3
Appendix E	The Shapiro-Loginov formula	S6
Appendix F	Decay Under Gaussian Noise	S13
Appendix G	The Smoothness of Decay Under Gaussian Noise	S16
Appendix H	Fitting to Many CPMG Curves Simultaneously	S16
Appendix I	Echoing Strongly Coupled Fluctuators	S16
Appendix J	Alternative Explanation of Coupler CPMG	S18

---

### Appendix A: Telegraph Noise

Here the statistics of a single random telegraph noise (RTN) process are briefly reviewed. The RTN process is a Markovian process in which the variable  $\xi(t)$  switches randomly between two values  $\xi(t) = \pm 1$  with an average rate  $\gamma$  [35]. We assume that the noise is symmetric, i.e. the probabilities of switching "up" and "down" are equal. The number of switches during time interval  $(0, t)$  is described by a Poisson distribution. As such, we can obtain the differential equation for the probability distribution of  $\xi(t)$ :

$$\frac{d}{dt} P_{\sigma_0, \sigma}^{\xi}(t) = -\gamma(P_{\sigma_0, \sigma}^{\xi}(t) - P_{\sigma_0, -\sigma}^{\xi}(t)) = -\gamma(2P_{\sigma_0, \sigma}^{\xi}(t) - 1) \quad (\text{A1})$$

Here  $P_{\sigma_0, \sigma}^{\xi}(t)$  is the probability that the discrete variable  $\xi(t)$  assumes the value  $\sigma$  conditioned on initial value  $\xi(0) = \sigma_0$  and we assumed that  $P_{\sigma_0, +}(t) + P_{\sigma_0, -}(t) = 1$ . For example,  $P_{+-}^{\xi}(t)$  is the probability that the variable  $\xi(t) = -1$  conditioned upon  $\xi(0) = +1$ . Eq. (A1) can be readily solved, and we obtain:

$$P_{\sigma_0, \sigma}^{\xi}(t) = \left( \delta_{\sigma_0, \sigma} - \frac{1}{2} \right) e^{-2\gamma t} + \frac{1}{2} \quad (\text{A2})$$

The two-point time-domain correlator of RTN and its Fourier transform can be obtained as well:

$$\langle \xi(t)\xi(0) \rangle = e^{-2\gamma|t|} \quad (\text{A3})$$

and

$$S(f) = \int_{-\infty}^{\infty} dt e^{i2\pi ft} \langle \xi(t)\xi(0) \rangle = \frac{\gamma}{\pi^2 f^2 + \gamma^2} \quad (\text{A4})$$

There also exists a useful recurrence relationship between higher order correlators and the second order correlator [35],

$$\langle \xi(t_1) \dots \xi(t_n) \rangle = \langle \xi(t_1)\xi(t_2) \rangle \langle \xi(t_3) \dots \xi(t_n) \rangle \quad (\text{A5})$$

or  $t_1 \geq t_2 > t_3, \dots, t_n$ .



### Appendix B: $1/f$ Noise From Telegraph Fluctuators

Consider the case of the noise that drives the qubit coming from the coupling to many independent random telegraph fluctuators. If the probability densities of the coupling strength  $\lambda$  and of the inverse correlation times of the fluctuators  $\gamma$  are  $g_\lambda(\lambda)$  and  $g_\gamma(\gamma)$ , respectively, the power spectrum of the noise is,

$$S(f) = \int_{-\infty}^{\infty} d\lambda g_\lambda(\lambda) \int_{-\infty}^{\infty} d\gamma g_\gamma(\gamma) \frac{\lambda^2 \gamma}{\pi^2 f^2 + \gamma^2} \quad (\text{B1})$$

In the particular case where  $\lambda$  is the same for all fluctuators,  $g_{\lambda_0}(\lambda_0) = \delta(\lambda_0 - \lambda)$ , and  $\gamma$  has a log-uniform density of states,

$$g_\gamma(\gamma) = \begin{cases} \frac{1}{(\ln(\gamma_{\max}) - \ln(\gamma_{\min}))\gamma}, & \gamma_{\min} < \gamma < \gamma_{\max} \\ 0, & \text{otherwise} \end{cases} \quad (\text{B2})$$

$S(f)$  takes the form,

$$S(f) = \lambda^2 \frac{\cot^{-1}\left(\frac{f\pi}{\gamma_{\max}}\right) - \cot^{-1}\left(\frac{f\pi}{\gamma_{\min}}\right)}{f\pi (\ln(\gamma_{\max}) - \ln(\gamma_{\min}))} \quad (\text{B3})$$

When  $\gamma_{\min} \ll f \ll \gamma_{\max}$ , the numerator is well approximated by  $\frac{\pi}{2}$ , and the noise spectrum is approximately  $S(f) = A/f$ . It should be noted that there are many possible other choices of  $g_\lambda(\lambda)$  and  $g_\gamma(\gamma)$  that yield a similar result.

### Appendix C: Flux Sensitivity in Tunable Coupler Systems

We are interested in understanding the dependance of the flux sensitivity  $\tilde{\chi}_\Phi$  on the coupling  $g$ . To do this we start with the formula for the total coupling  $g$  between the qubits:

$$g = \left( k_d - k^2 \frac{\omega_q^2}{\omega_c^2 - \omega_q^2} \right) \frac{\omega_q}{2}, \quad (\text{C1})$$

where  $\omega_q$  is the qubit frequency (we assume that both qubits are on resonance),  $k_d$  and  $k^2$  are dimensionless parameters that we will call coupling efficiencies. These parameters can be expressed through effective capacitances of the qubit-coupler system [24].  $\omega_c$  is the coupler frequency:

$$\omega_c \simeq \frac{1}{\hbar} \left( \sqrt{8E_J E_C |\cos(\pi\Phi/\Phi_0)|} - E_C \right) \simeq \omega_{\max} \sqrt{|\cos(\pi\Phi/\Phi_0)|}, \quad (\text{C2})$$

where  $E_J$  and  $E_C$  are the Josephson and charging energies respectively and  $\omega_{\max}$  is the frequency of a tunable transmon at the flux insensitive point  $\Phi = 0$ . Expression (C2) is valid if the strong inequality  $E_J/E_C \gg 1$  is satisfied. Using Eqs. (C1) and (C2) we can express the flux sensitivity as

$$\tilde{\chi}_\Phi = \left| \frac{\partial g}{\partial \Phi} \right| = \frac{k^2 \omega_q^3 \omega_{\max}^2 \sin(\pi\Phi/\Phi_0)}{4\Phi_0 (\omega_{\max}^2 \cos(\pi\Phi/\Phi_0) - \omega_q^2)^2} \quad (\text{C3})$$

Solving the system of equations (C1) and (C2) for  $\Phi$  and  $\omega_c$  and substituting the result into Eq. (C3) we obtain the desired relation between the flux sensitivity and  $g$ :

$$\tilde{\chi}_\Phi(g) = \frac{(k_d \omega_q - 2g) \sqrt{\omega_{\max}^4 (k_d \omega_q - 2g)^2 - \omega_q^4 (k_{qq} \omega_q - 2g)^2}}{4\Phi_0 k^2 \omega_q^3}, \quad (\text{C4})$$

where  $k_{qq} = k_d + k^2$  is the total coupling efficiency, which includes both direct and indirect interactions between the qubits. The flux sensitivity in (C4) is positive since we are considering only those  $\omega_c$  for which the indirect coupling

prevails, i.e. according to Eq. (C1) the value of  $g$  is negative; we also assume  $\omega_c > \omega_q$ . In the parameter range of interest for the experiment, and in particular with the account taken of the smallness of the dimensionless parameter  $k$ ,  $\tilde{\chi}_\Phi(g)$  is extremely well approximated by a quadratic polynomial in  $g$  as  $\tilde{\chi}_\Phi(g) = \chi_\Phi^{(0)} + \chi_\Phi^{(1)}g + \chi_\Phi^{(2)}g^2$ . We note that in the vicinity of  $g = 0$  the  $g$ -noise is negligible and the total qubit dephasing time  $T_\varphi$  is dominated by other noise sources. As such, we will treat the first term  $\chi_\Phi^{(0)}$  of the polynomial as a free parameter.

#### Appendix D: Direct averaging over Noise Trajectories

Here the average of the stochastic dynamics of the qubit will be found by first analytically solving for the dynamics for a single trajectory of the RTN and then directly averaging over all possible trajectories.

First, we will consider the case of Coupler Ramsey decay under noise described by a single RTN process entering through the flux bias of the coupler. If the frequencies of the both qubits coincide, the complete Hamiltonian is,

$$H(t) = (g(t) + \lambda(t)\xi(t))\sigma_x \quad (\text{D1})$$

Here,  $g(t)$  is a periodic sequence of pulses with period  $T_{\text{gate}}$ . From the analysis completed in section C, this also implies that  $\lambda(t)$  is periodic with the same period. The associated propagator is,

$$U(t) = e^{-i\sigma_x G(t,0)} \quad (\text{D2})$$

$$G(t_2, t_1) = \int_{t_1}^{t_2} [g(\tau) + \lambda(\tau)\xi(\tau)]d\tau \quad (\text{D3})$$

If the system is initialized in the state  $\rho(0) = |01\rangle\langle 01|$ , the z-component of the one-excitation subspace Bloch vector  $N(t) \equiv \text{Tr}[\sigma_z \rho(t)]$  is given by the expression

$$\begin{aligned} N(t) &= \langle 01|U(t)\rho(0)U^\dagger(t)|01\rangle - \langle 10|U(t)\rho(0)U^\dagger(t)|10\rangle \\ &= \text{Re}(e^{2i\int_0^t \lambda(\tau)\xi(\tau)d\tau} e^{2i\int_0^t g(\tau)d\tau}) \end{aligned} \quad (\text{D4})$$

The average Bloch vector component can be found by averaging Eq. D4 over noise trajectories. Taking into account that the measurement is done after an even number of  $g$ -gates,  $\int_0^t g(t')dt' k\pi$ , we have

$$\langle N(t) \rangle = \text{Re} \left( \chi(t) e^{2i\int_0^t g(\tau)d\tau} \right) \quad (\text{D5})$$

$$\chi(t) = \langle e^{2i\int_0^t \lambda(\tau)\xi(\tau)d\tau} \rangle \quad (\text{D6})$$

The averaging can be accomplished by expanding the functional  $\chi(t)$  in a time-ordered Taylor series

$$\chi(t) = \sum_{k=0}^{\infty} (2i)^k \int_0^t dt_1 \int_0^{t_1} dt_2 \cdots \int_0^{t_{k-1}} dt_k \langle \xi(t_1) \dots \xi(t_k) \rangle \lambda(t_1) \dots \lambda(t_k) \quad (\text{D7})$$

In the considered problem  $\lambda(t)$  is a periodic function of time. The typical period is the periodicity of the gate (moreover,  $\lambda(t)$  is very nonsinusoidal, for much of the gate duration it is constant). The period of  $\lambda(t)$  is much shorter than the typical time on which  $\chi(t)$  varies. Therefore the major contribution to  $\chi(t)$  comes from the term in  $\lambda(t)$  that is independent of time. A justification of approximating  $\lambda(t)$  by a constant can be done using the master equation formulation in Sec. V. One can see there that the fast-oscillating terms in  $\lambda(t)$  lead to fast oscillating terms in the density matrix, which are small.

For  $\lambda(t) \equiv \lambda = \frac{1}{t_g} \int_0^{t_g} \lambda(\tau)d\tau$  we can use the recurrence relation for the moments given in Eq. A5 to find a second order linear differential equation for  $\chi(t)$ ,

$$\frac{d^2\chi(t)}{dt^2} + 2\gamma\frac{d\chi(t)}{dt} + 4\lambda^2\chi(t) = 0 \quad (\text{D8})$$

We can infer the initial conditions  $\chi(0) = 1$  and  $\chi'(0) = 0$  from Eq. D7. Then

$$\chi(t) = e^{-\gamma t} \left( \cosh(t\Omega) + \frac{\gamma \sinh(t\Omega)}{\Omega} \right) \quad (\text{D9})$$

$$\Omega = \sqrt{\gamma^2 - 4\lambda^2} \quad (\text{D10})$$

We can now consider the case of Coupler-CPMG decay. Here we apply a periodic sequence of  $\sigma_z$  gates to suppress the coupler noise. In the limit that the  $\sigma_z$  gates are very short, the Hamiltonian that describes the Coupler-CPMG reads:

$$H_{\text{CPMG}} = H(t) - \frac{\pi}{2}\sigma_z \sum_k \delta[t - (k + 1/2)T_C] \quad (\text{D11})$$

Here the period  $T_C$  is the duration of a sequence of  $2m$  two-qubit gates. The pulses  $\propto \sigma_z$  are the pulses of the difference of the qubit frequencies, and during these pulses in the experiment  $g(t) = 0$ , so that the coupled noise is not accumulated. As in the conventional CPMG, the first refocusing pulse is applied at  $T_C/2$ , and the measurement is at  $nT_C$ , that is, the time interval between the last refocusing pulse and the measurement is  $T_C/2$ .

The time evolution operator of the system is

$$U_{\text{CPMG}}(nT_C, 0) = \mathcal{T} \exp \left[ -i \int_0^{nT_C} dt H_{\text{CPMG}}(t) \right] \quad (\text{D12})$$

( $\mathcal{T}$  is the time ordering operator). The operator  $U_{\text{CPMG}}$  can be simplified if one takes into account that  $\sigma_z\sigma_x = -\sigma_x\sigma_z$ , and therefore  $\sigma_z \exp[-i \int H(t)dt] = \exp[i \int H(t)dt]\sigma_z$ . One can then use in Eq. (D12) that  $\exp(-i\pi\sigma_z/2) = -i\sigma_z$  and move in the time-ordered operator  $U_{\text{CPMG}}$  all  $\sigma_z$  at times  $(2k + 1)T_C$  to  $(2k + 2)T_C$  ( $k = 0, \dots, \lfloor (n - 2)/2 \rfloor$ ); for odd  $n - 1$  the last  $\sigma_z$  is moved to  $nT_C$ . This gives

$$U_{\text{CPMG}}(nT_C) = (-i)^{n-1} \exp \left[ -i \int_0^{nT_C} h(t)H(t) \right], \quad (\text{D13})$$

where  $h(t)$  is a filter function. It changes sign depending on  $t$  being in the interval preceded by an even or odd number of refocusing pulses,

$$h(t) = 1 + 2 \sum_{m=1}^n (-1)^m \Theta[t - (m - 1/2)T_C] \quad (\text{D14})$$

We now consider the expectation value of the z-component of the Bloch vector  $N_{\text{CPMG}}(nT_C) = \langle \text{Tr}[\sigma_z U_{\text{CPMG}}(nT_C)\rho(0)U_{\text{CPMG}}^\dagger(nT_C)] \rangle$ . Taking into account that  $[H(t), H(t')] = 0$ , we can write the general expression for the observable in the form similar to that in the absence of the CPMG pulses

$$N_{\text{CPMG}}(nT_C) = \text{Re}(\chi_{\text{CPMG}}(nT_C)) \quad (\text{D15})$$

where

$$\chi_{\text{CPMG}}(t) = \langle e^{2i \int_0^t h(\tau)\lambda(\tau)\xi(\tau)d\tau} \rangle \quad (\text{D16})$$

There are several ways to calculate the average (D16). They take advantage of  $\xi(t)$  being a Markov random process and of the property (A5). Here we start by employing time ordered expansion of the telegraph noise to find an integro-differential equation for  $\chi_{\text{CPMG}}(t)$ ,

$$\frac{d\chi_{\text{CPMG}}(t)}{dt} = -4\lambda(t)h(t) \int_0^t e^{-2\gamma(t-t_1)} \lambda(t_1)h(t_1)\chi_{\text{CPMG}}(t_1)dt_1 \quad (\text{D17})$$

We define  $\Lambda(t)$ ,

$$\Lambda(t) = 2 \int_0^t e^{-2\gamma(t-t_1)} \lambda(t_1)h(t_1)\chi_{\text{CPMG}}(t_1)dt_1 \quad (\text{D18})$$

and arrive at the system of equations,

$$\begin{aligned} \frac{d}{dt} \begin{pmatrix} \chi_{\text{CPMG}}(t) \\ \Lambda(t) \end{pmatrix} &= A(t) \begin{pmatrix} \chi_{\text{CPMG}}(t) \\ \Lambda(t) \end{pmatrix} \\ A(t) &= \begin{pmatrix} 0 & -2\lambda(t)h(t) \\ 2\lambda(t)h(t) & -2\gamma \end{pmatrix} \end{aligned} \quad (\text{D19})$$

Given that we consider the case  $\lambda(t)=\text{const}$  and  $h(t) = \pm 1$ , the solution of Eq. (D19) can be obtained using the transfer matrix approach based on the piece-wise solution within an interval where  $h(t) = \text{const}$ .

For  $h = 1$  we have

$$\begin{aligned} \begin{pmatrix} \chi_{\text{CPMG}}(t) \\ \Lambda(t) \end{pmatrix} &= \hat{X}_{h=1}(t-t_1) \begin{pmatrix} \chi_{\text{CPMG}}(t_1) \\ \Lambda(t_1) \end{pmatrix}, \\ \hat{X}_{h=1}(t) &= e^{-\gamma t} \begin{pmatrix} \cosh(\Omega t) + \frac{\gamma}{\Omega} \sinh(\Omega t) & -\frac{2\lambda \sinh(\Omega t)}{\Omega} \\ \frac{2\lambda \sinh(\Omega t)}{\Omega} & \cosh(\Omega t) - \frac{\gamma}{\Omega} \sinh(\Omega t) \end{pmatrix}, \end{aligned} \quad (\text{D20})$$

where  $\Omega$  is given by Eq. D10.

The solution of Eq. (D19) for  $h = -1$  has the same form, except that  $X_{h=1}$  has to be replaced with  $\hat{X}_{h=-1}$ . The expression for  $\hat{X}_{h=-1}$  can be obtained from Eq. (D20) by replacing  $\lambda \rightarrow -\lambda$ . Alternatively, it can be written as

$$\hat{X}_{h=-1}(t) = \hat{Z} \hat{X}_{h=1}(t) \hat{Z}, \quad \hat{Z} = \begin{pmatrix} 1 & 0 \\ 0 & -1 \end{pmatrix} \quad (\text{D21})$$

The introduction of the matrix  $\hat{Z}$  and the form of the solution for  $h = \pm 1$  allows us to write the expression for the function  $\chi_{\text{CPMG}}(nT_C)$  in the form

$$\chi_{\text{CPMG}}(nT_C) = \begin{pmatrix} 1 & 0 \end{pmatrix} \hat{Z}^{(n \bmod 2)} \left( \hat{X}_{h=1}(T_C/2) \hat{Z} \hat{X}_{h=1}(T_C/2) \right)^n \begin{pmatrix} 1 \\ 0 \end{pmatrix} \quad (\text{D22})$$

We have

$$\hat{X}_{h=1}(T_C/2) \hat{Z} \hat{X}_{h=1}(T_C/2) = e^{-\gamma T_C} \begin{pmatrix} (\gamma/\Omega) \sinh \Omega T_C + q & -(4\lambda\gamma/\Omega^2) \sinh^2(\Omega T_C/2) \\ (4\lambda\gamma/\Omega^2) \sinh^2(\Omega T_C/2) & (\gamma/\Omega) \sinh \Omega T_C - q \end{pmatrix}, \quad (\text{D23})$$

where

$$q = \frac{-4\lambda^2}{\Omega^2} + \frac{\gamma^2 \cosh(\Omega T_C)}{\Omega^2} \quad (\text{D24})$$

The matrix (D23) is not skew-Hermitian, although the off-diagonal matrix elements have opposite signs, since  $\Omega$  is either real or imaginary. Therefore its eigenvectors are not orthogonal.

The eigenvalues of the matrix  $XZX$  are  $-e^{-\alpha}$  and  $e^\alpha$  where  $\alpha$  is a solution of the equation

$$\sinh \alpha = \frac{\gamma}{\Omega} \sinh \Omega T_C \quad (\text{D25})$$

The expression for  $\chi_{\text{CPMG}}$  is then easily found,

$$\chi_{\text{CPMG}}(nT_C) = \begin{cases} e^{-n\gamma T_C} \left( q \frac{\cosh(n\alpha)}{\cosh(\alpha)} + \sinh(n\alpha) \right), & \text{n odd} \\ e^{-n\gamma T_C} \left( q \frac{\sinh(n\alpha)}{\cosh(\alpha)} + \cosh(n\alpha) \right), & \text{n even} \end{cases} \quad (\text{D26})$$

It is clear how to extend the results to a superposition of independent RTN processes. For example, in the case of CPMG evolution,

$$\begin{aligned} \chi_{\text{CPMG}}(t) &= \langle e^{2i \int_0^t h(\tau) \sum_k \lambda_k(\tau) \xi_k(\tau) d\tau} \rangle \\ &= \prod_k \langle e^{2i \int_0^t h(\tau) \lambda_k(\tau) \xi_k(\tau) d\tau} \rangle \\ &= \prod_k \chi_{\text{CPMG}}^{(k)}(t) \end{aligned} \quad (\text{D27})$$

with  $\chi_{\text{CPMG}}^{(k)}(nT_C)$  given by Eq. (D26) for the parameters  $\gamma, \lambda$  referred to the  $k$ th fluctuator.

If we set in Eq. (D27)  $h(t) = 1$ , it describes the result in the absence of refocusing pulses.

### Appendix E: The Shapiro-Loginov formula

The direct averaging approach used in section D is useful when a simple, closed form solution for single trajectories of the noise is available. When this is not possible, other techniques must be used. One example of such a technique is the Shapiro-Loginov formula, which is valid for random processes with exponential correlators:

$$\langle \xi(t) \frac{d}{dt} R[\xi(t), t] \rangle = \frac{d}{dt} \langle \xi(t) R[\xi(t), t] \rangle + 2\gamma \langle \xi(t) R[\xi(t), t] \rangle \quad (\text{E1})$$

Here  $R[\xi(t), t]$  is any functional of all histories  $\{\xi(t'), t' \leq t\}$  that lead to value  $\xi(t') = \xi(t)$  at  $t' = t$  and the angular brackets mean averaging over all possible noise instances.

First we consider the case of Coupler Ramsey decay. Let us write the Liouville - Von Neumann equation for the evolution of a density matrix of a qubit under a single source of the telegraph noise, and average over the noise instances using Shapiro-Loginov formula. We write this equation in the vectorized form, which for a two-level system is a well known Bloch equation for three components of the Bloch vector. For a two-qubit system in a single excitation subspace the x,y and z components are respectively:  $P(t) = \langle 01 | \rho | 10 \rangle + \langle 10 | \rho | 01 \rangle$ ,  $Q(t) = i(\langle 01 | \rho | 10 \rangle - \langle 10 | \rho | 01 \rangle)$  and  $N(t) = \langle 01 | \rho | 01 \rangle - \langle 10 | \rho | 10 \rangle$ . The Bloch equation reads:

$$\dot{\rho}(t) = (L_q(t) + \lambda(t)\xi(t)L_x)\rho(t) \quad (\text{E2})$$

where

$$L_q(t) = \begin{pmatrix} 0 & \omega(t) & 0 \\ -\omega(t) & 0 & g(t) \\ 0 & -g(t) & 0 \end{pmatrix} \quad (\text{E3})$$

is the regular part of the Liouvillian with  $\omega(t)$  and  $g(t)$  being the detuning and coupling between the qubits, respectively. The second term represents a stochastic part of the Liouvillian and describes coupling of the qubit with the noise of amplitude  $\lambda(t)$ . The operator

$$L_x = \begin{pmatrix} 0 & 0 & 0 \\ 0 & 0 & 1 \\ 0 & -1 & 0 \end{pmatrix} \quad (\text{E4})$$

represents the noise coupling. The important property of the telegraph noise is that  $\xi^2(t) = 1$ , which substantially simplifies calculations. The second simplification comes from the Shapiro-Loginov formula. As a first step, we average the Liouville equation and obtain:

$$\frac{d}{dt} \langle \rho(t) \rangle = L_q(t) \langle \rho(t) \rangle + \lambda(t) L_x \langle \xi(t) \rho(t) \rangle \quad (\text{E5})$$



Now we need to come up with an equation for  $\mu(t) = \langle \xi(t)\rho(t) \rangle$ . To obtain this equation we multiply the Bloch equation (E2) by  $\xi(t)$  and replace  $\langle \xi(t)\dot{\rho}(t) \rangle$  using Shapiro-Loginov formula (E1). After multiplication by  $\xi(t)$  the second term in Eq. (E2) will be proportional to  $\langle \rho(t) \rangle \times \text{const}$  because  $\xi^2(t) = 1$ . This yields

$$\frac{d}{dt}\mu(t) + 2\gamma\mu(t) = L_q(t)\mu(t) + \lambda(t)L_x\langle\rho(t)\rangle \quad (\text{E6})$$

Therefore we obtained a closed system of linear differential equations which can be expressed compactly in a matrix form as

$$\begin{pmatrix} \dot{\rho}(t) \\ \dot{\mu}(t) \end{pmatrix} = \mathcal{L}(t) \begin{pmatrix} \rho(t) \\ \mu(t) \end{pmatrix} \quad (\text{E7})$$

where

$$\mathcal{L}(t) = \begin{pmatrix} L_q(t) & \lambda(t)L_x \\ \lambda(t)L_x & L_q(t) - 2\gamma I_q \end{pmatrix} \quad (\text{E8})$$

is  $6 \times 6$  matrix comprised of four  $3 \times 3$  blocks,  $I_q$  is a  $3 \times 3$  unit matrix. The system of linear differential equations (E7) must be solved with the initial conditions  $\mu(0) = \langle \xi(0)\rho(0) \rangle = \langle \xi(0) \rangle \langle \rho(0) \rangle = 0$ . From now on we will omit angular brackets for averaged quantities and assume that  $\rho(t)$  is the averaged density matrix (like in Eq. (E7)) unless specified otherwise.

It is seen from this equation that, as mentioned earlier, if  $\lambda(t)$  has an oscillating component with typical period  $T_\lambda \ll \gamma^{-1}, |\lambda|^{-1}$ , this component leads to the terms in  $\rho(t), \mu(t)$  oscillating with the same period. The amplitude of these terms is  $\propto (\gamma T)^{-1}, |\lambda T|^{-1} \ll 1$ . This justifies keeping only the time-independent term in  $\lambda$ .

The Liouvillian  $\mathcal{L}(t)$  can be expressed in the operator form using Pauli matrices:

$$\mathcal{L}(t) = I_2 \otimes L_q(t) + \lambda \sigma_x \otimes L_x + \gamma (\sigma_z - I_2) \otimes I_q \quad (\text{E9})$$

This form will be important for generalization to a multi-fluctuator case. Let us split Liouvillian (E9) into two parts such that  $\mathcal{L} = \mathcal{L}_q + \mathcal{L}_{noise}$ , where  $\mathcal{L}_q$  is the first term in Eq. (E9) and  $\mathcal{L}_{noise}$  is the sum of the second and third terms. If  $\omega(t) = 0$  the matrices  $\mathcal{L}_q$  and  $\mathcal{L}_{noise}$  commute and can be diagonalized separately.

$$\varrho(t) = e^{\mathcal{L}_q G(t)} e^{\mathcal{L}_{noise} t} \varrho(0) \quad (\text{E10})$$

$$G(t) = \int_0^t g(\tau) d\tau \quad (\text{E11})$$

Here  $\varrho(t)$  is the generalized density matrix such that  $\varrho^T(t) = (\rho(t), \mu(t))$ . The Liouvillian  $\mathcal{L}_q$  describes uniform rotation of the Bloch vector in  $yz$  plane while  $\mathcal{L}_{noise}$  describes its dynamics in the corresponding rotating frame. The explicit form of the matrix matrix  $\mathcal{L}_{noise}$  is:

$$\mathcal{L}_{noise} = 2 \begin{pmatrix} -\gamma & 0 & 0 & 0 & 0 & 0 \\ 0 & -\gamma & 0 & 0 & 0 & -\lambda \\ 0 & 0 & -\gamma & 0 & \lambda & 0 \\ 0 & 0 & 0 & 0 & 0 & 0 \\ 0 & 0 & -\lambda & 0 & 0 & 0 \\ 0 & \lambda & 0 & 0 & 0 & 0 \end{pmatrix} \quad (\text{E12})$$

The eigenvalues and eigenvectors of  $\mathcal{L}_{noise}$  can be obtained by solving two quadratic equations. As a result, for the initial condition  $N(0) = 1$  we obtain:

$$N(t) = \cos(2G(t))\chi(t) \quad (\text{E13})$$

$$Q(t) = \sin(2G(t))\chi(t) \quad (\text{E14})$$

$$P(t) = 0 \quad (\text{E15})$$

where

$$\chi(t) = e^{-\gamma t} \left( \cosh(\Omega t) + \frac{\gamma}{\Omega} \sinh(\Omega t) \right) \quad (\text{E16})$$

Where  $\Omega$  is as given in Eq. D10. As required, this solution is identical to that found using the direct averaging approach.

The solution in the case of CPMG decay is found nearly identically to that in the case of Coupler Ramsey decay. It is most convenient to break the evolution into stages. Identically to the previous section, we can use the Shapiro-Loginov equation to find the evolution during  $g$  pulses for the generalized density matrix  $\varrho$ ,

$$\frac{d\varrho}{dt} = (iH_G(t) + L_G)\varrho \quad (\text{E17})$$

Where  $H_G(t)$  represents the driving from the coupler and  $L_G$  the coupler noise. These matrices commute, so the solution is given in terms of two commuting propagators,

$$\varrho(t + T_G) = X_G U_G \varrho(t) \quad (\text{E18})$$

As above, the eigenvectors of  $H_G(t)$  are time independent, so the propagator is found easily. Similarly, the evolution during the frequency pulses is given by,

$$\varrho(t + T_P) = X_P U_P \varrho(t) \quad (\text{E19})$$

We know that the coupler noise is approximately zero when the coupler is off, so the operator  $U_P$  represents the frequency pulse itself and  $X_P$  represents the evolution of the uncoupled fluctuator during the pulse. Therefore, we can write the solution after  $n$  repetitions of the drive pulse via,

$$\varrho(nT_C) = (X_G U_G X_P U_P X_G U_G)^n \varrho(0) \quad (\text{E20})$$

In the case where  $U_P$  is a  $\pi$  pulse and  $T_P \rightarrow 0$ , the above matrix reduces to a block diagonal form where at most 2 elements are coupled to each other. The evolution of the  $z$  component of the Bloch vector is given by,

$$\frac{d}{dt} \begin{pmatrix} \langle N(t) \rangle \\ \langle \xi(t) P(t) \rangle \end{pmatrix} = (XZX)^n \begin{pmatrix} \langle N(t) \rangle \\ \langle \xi(t) P(t) \rangle \end{pmatrix} \quad (\text{E21})$$

Where  $P(t)$  is the  $x$ -component of the Bloch vector, and the matrix  $XZX$  identical to the one found in Eq. D22. The solution is then also given by Eq. D26, as required.

The problem of many fluctuators coupling to a single qubit must also be considered. Before we proceed with this we need to investigate statistical properties of a product of many RTN variables  $\xi_1(t)\xi_2(t)\dots\xi_N(t)$ . Let us consider a product of two independent telegraph variables  $\xi(t) = \xi_1(t)\xi_2(t)$  and find its distribution based on the distributions of  $\xi_1(t)$  and  $\xi_2(t)$ . It is sufficient to concentrate on only one initial condition, e.g.  $\xi(0) = +1$ . Based on the probability calculus for discrete and independent random variables we can express the probabilities  $P_{++}^\xi(t)$  and  $P_{+-}^\xi(t)$  as follows:

$$P_{++}^\xi(t) = \frac{1}{2} \left( P_{++}^{\xi_1}(t) P_{++}^{\xi_2}(t) + P_{--}^{\xi_1}(t) P_{--}^{\xi_2}(t) + P_{+-}^{\xi_1}(t) P_{+-}^{\xi_2}(t) + P_{-+}^{\xi_1}(t) P_{-+}^{\xi_2}(t) \right) \quad (\text{E22})$$

$$P_{+-}^\xi(t) = \frac{1}{2} \left( P_{++}^{\xi_1}(t) P_{+-}^{\xi_2}(t) + P_{--}^{\xi_1}(t) P_{-+}^{\xi_2}(t) + P_{+-}^{\xi_1}(t) P_{++}^{\xi_2}(t) + P_{-+}^{\xi_1}(t) P_{--}^{\xi_2}(t) \right), \quad (\text{E23})$$

where the factor  $1/2$  is due to the fact that there are two equally probable and indistinguishable cases ( $\xi_1(0), \xi_2(0) = +1, +1$  and  $\xi_1(0), \xi_2(0) = -1, -1$ ) satisfying initial condition  $\xi(0) = +1$ , and the distributions functions for individual fluctuators are:

$$P_{\sigma_0, \sigma}^{\xi_i}(t) = \frac{1}{2} + \left( \delta_{\sigma_0, \sigma} - \frac{1}{2} \right) e^{-2\gamma_i t} \quad (\text{E24})$$

Substitution of Eq. (E24) into Eqs. (E22) and (E23) yields:

$$P_{++}^\xi(t) = \frac{1}{2} \left( 1 + e^{-2(\gamma_1 + \gamma_2)t} \right) \quad (\text{E25})$$

$$P_{+-}^\xi(t) = \frac{1}{2} \left( 1 - e^{-2(\gamma_1 + \gamma_2)t} \right) \quad (\text{E26})$$

Eqs. (E25) and (E26) ensure that any product of independent telegraph variables is also a telegraph variable with the switching rate  $\gamma = \sum_i \gamma_i$ . As such, we can apply Shapiro-Loguinov formula to a product of any number of telegraph variables and repeat the procedure described in the previous section.

Now we are ready to describe a set of  $M$  fluctuators coupled to our two-qubit system. To understand the structure of the master equations let us imagine that  $L_q = 0$  and both  $L_x$  and  $L_q$  are scalars. We make these assumptions only for instructive purposes because they are nonsensical in the context of Bloch equations. For the sake of simplicity we assume that  $M = 2$ . Repeating the single fluctuator procedure described above, i.e. multiplying "master equations" sequentially by  $\xi_1(t)$ ,  $\xi_2(t)$ , and  $\xi_1(t)\xi_2(t)$ , using  $\xi_i^2(t) = 1$  and applying Shapiro-Loguinov formula we obtain:

$$\frac{d}{dt} \begin{pmatrix} \rho \\ \mu_1 \\ \mu_2 \\ \mu_{12} \end{pmatrix} = \begin{pmatrix} 0 & \lambda_2 & \lambda_1 & 0 \\ \lambda_2 & -2\gamma_2 & 0 & \lambda_1 \\ \lambda_1 & 0 & -2\gamma_1 & \lambda_2 \\ 0 & \lambda_1 & \lambda_2 & -2\gamma_1 - 2\gamma_2 \end{pmatrix} \begin{pmatrix} \rho \\ \mu_1 \\ \mu_2 \\ \mu_{12} \end{pmatrix} \quad (\text{E27})$$

where  $\mu_1(t) = \langle \xi_1(t)\rho(t) \rangle$ ,  $\mu_2(t) = \langle \xi_2(t)\rho(t) \rangle$  and  $\mu_{12}(t) = \langle \xi_1(t)\xi_2(t)\rho(t) \rangle$ . It is straightforward now to rewrite the matrix in Eq. (E27) in the operator form:

$$\mathcal{L} = \lambda_1 \sigma_x \otimes I_2 + \lambda_2 I_2 \otimes \sigma_x + 2\gamma_1 \sigma_z \otimes I_2 + 2\gamma_2 I_2 \otimes \sigma_z - 2(\gamma_1 + \gamma_2) I_4 \quad (\text{E28})$$

As such we can associate the matrices  $\sigma_\alpha \otimes I_2$  and  $I_2 \otimes \sigma_\alpha$  with fluctuators 1 and 2 respectively. Generalization to any number of fluctuators and any qubit Liouvillian is straightforward and we arrive at the following Liouvillian of the system of  $M$  fluctuators coupled to a two-qubit system:

$$\mathcal{L} = I_{2M} \otimes L_q(t) + \sum_{i=1}^M \lambda_i \sigma_x(i) \otimes L_x + \sum_{i=1}^M \gamma_i (\sigma_z(i) - I_{2M}) \otimes I_d, \quad (\text{E29})$$

where

$$\sigma_\alpha(i) = I_2 \otimes I_2 \otimes \cdots \otimes \sigma_\alpha \otimes \cdots \otimes I_2 \quad (\text{E30})$$

and the Pauli matrix  $\sigma_\alpha$  is exactly at  $i_{th}$  position in this product. Eq. (E29) can be interpreted as a central spin problem describing Ising-type interaction of the individual fluctuators (peripheral spins) with the two-qubit system (central spin). In the case  $\Delta(t) = 0$  when the qubit Liouvillian commutes with the noise Hamiltonian this problem can be solved exactly.

At first, one need to transform equations of motion to a rotating frame associated with  $g$ . Then in the absence of the the z-component of the magnetic field ( $\Delta(t) = 0$ ) the fluctuators do not interact with each other and eigenvalues of the operator  $L_x$  are good quantum numbers. As such, each peripheral spin senses only the local "magnetic field" with  $x$ -component 0, or  $\pm 4\pi\lambda_i$ , imaginary  $z$ -component  $2i\gamma_i$ . Therefore the Liouvillian can be diagonalized by rotating quantization axis of each spin to a local frame defined by this magnetic field. Since one of the filed components is imaginary this transformation is described by a hyperbolic rotation for each qubit:

$$z_i = \begin{pmatrix} \cosh\left(\frac{\beta_i}{2}\right) & i \sinh\left(\frac{\beta_i}{2}\right) \\ -i \sinh\left(\frac{\beta_i}{2}\right) & \cosh\left(\frac{\beta_i}{2}\right) \end{pmatrix}, \quad (\text{E31})$$

where

$$\cosh(\beta_i) = \frac{\gamma_i}{\sqrt{\gamma_i^2 - 16\pi^2\lambda_i^2}} \quad (\text{E32})$$

To diagonalize the Liouvillian (E29) we construct  $2^M \times 2^M$  rotation matrices

$$\zeta(i) = I_2 \otimes I_2 \otimes \cdots \otimes z_i \otimes \cdots \otimes I_2 \quad (\text{E33})$$

where  $z_i$  is at  $i_{th}$  position in this product. It is convenient to rewrite Eq. (E29) as

$$\mathcal{L}_r(t) = L_q(t) \otimes I_{2^M} + L_x \otimes \sum_{i=1}^M \lambda_i \sigma_x(i) + I_d \otimes \sum_{i=1}^M \gamma_i (\sigma_z(i) - I_{2^M}), \quad (\text{E34})$$

which corresponds to the master equation

$$\dot{\varrho}(t) = \varrho(t) \mathcal{L}_r(t) \quad (\text{E35})$$

Then we diagonalize  $L_x$  to separate the blocks corresponding to its eigenvalues  $\pm i$  and 0. The transformation, which completely diagonalizes  $\mathcal{L}_r(t)$  in the rotating frame takes the form:

$$\mathcal{L}_{diag} = Z^\dagger \mathcal{U}_x^\dagger \mathcal{L}_r \mathcal{U}_x Z, \quad (\text{E36})$$

where

$$Z = (P_+ + P_-) \otimes \prod_{i=1}^M \zeta(i) + P_0 \otimes I_{2^M}, \quad (\text{E37})$$

$P_\pm$  and  $P_0$  are the projectors onto the eigenstates of  $L_x$  with eigenvalues  $\pm i$  and 0, respectively,  $\mathcal{U}_x = u_x \otimes I_{2^M}$  and

$$u_x = \begin{pmatrix} 0 & 0 & 1 \\ -\frac{i}{\sqrt{2}} & \frac{i}{\sqrt{2}} & 0 \\ \frac{1}{\sqrt{2}} & \frac{1}{\sqrt{2}} & 0 \end{pmatrix} \quad (\text{E38})$$

is the matrix diagonalizing  $L_x$ . After this transformation the problem is reduced to solving  $3 \times 2^M$  linear differential equations and the final result corresponding to the initial condition  $N(0) = 1$  reads:

$$N(t) = \cos(2G(t))\chi(t) \quad (\text{E39})$$

$$Q(t) = \sin(2G(t))\chi(t) \quad (\text{E40})$$

$$P(t) = 0 \quad (\text{E41})$$

where

$$\chi(t) = \prod_k e^{-\gamma_k t} \left( \cosh(\Omega_k t) + \frac{\gamma_k}{\Omega_k} \sinh(\Omega_k t) \right) \quad (\text{E42})$$

In real experiments, there is noise present other than the coupler noise we are focused on. For example, independent single qubit decay and dephasing may contribute significantly to what is seen in experimental measurements. Single qubit decay and dephasing can be modeled alongside classical coupler noise via the Lindblad equation,

$$\begin{aligned} \frac{d\rho}{dt} &= -i[H(t), \rho] + L_t[\rho] + L_l[\rho] \\ L_t[\rho] &= \sum_{m=1}^2 \Gamma_m^\phi \left( n_m n_m \rho(t) - \frac{1}{2} \{n_m n_m, \rho(t)\} \right) \\ L_l[\rho] &= \sum_{m=1}^2 \Gamma_m^1 \left( \sigma_m^- \rho(t) \sigma_m^+ - \frac{1}{2} \{ \rho(t), \sigma_m^+ \sigma_m^- \} \right) \end{aligned} \quad (\text{E43})$$

Where  $n_m$  is the number operator for qubit m and  $\sigma_m^-$  and  $\sigma_m^+$  are the annihilation and creation operators for qubit m, respectively. First we will focus on the free evolution problem. It is most convenient to divide the total Hamiltonian (D1) into two parts,

$$\begin{aligned} H(t) &= H_C(t) + H_N(t) \\ H_C(t) &= g(t) \sigma_x \\ H_N(t) &= \lambda(t) \xi(t) \sigma_x \end{aligned} \quad (\text{E44})$$

Let  $U_C(t)$  be the unitary generated by  $H_C$ .

$$\begin{aligned} U_C(t) &= e^{-i\sigma_x G(t)} \\ G(t) &= \int_0^t g(\tau) d\tau \end{aligned} \quad (\text{E45})$$

Eq. E43 can then be moved into the interaction picture of  $U_C(t)$ . Defining  $\tilde{\rho} = U_C^\dagger \rho U_C$  and noting that  $[U_C, H_N] = 0$ ,

$$\begin{aligned} \frac{d\tilde{\rho}}{dt} &= -i[H_N(t), \tilde{\rho}] + \tilde{L}_t[\tilde{\rho}] + \tilde{L}_l[\tilde{\rho}] \\ \tilde{L}_t[\tilde{\rho}] &= \sum_{m=1}^2 \Gamma_m^\phi \left( \tilde{n}_m \tilde{n}_m \tilde{\rho} - \frac{1}{2} \{ \tilde{n}_m \tilde{n}_m, \tilde{\rho} \} \right) \\ \tilde{L}_l[\tilde{\rho}] &= \sum_{m=1}^2 \Gamma_m^1 \left( \tilde{\sigma}_m^- \tilde{\rho} \tilde{\sigma}_m^+ - \frac{1}{2} \{ \tilde{\rho}, \tilde{\sigma}_m^+ \tilde{\sigma}_m^- \} \right) \end{aligned} \quad (\text{E46})$$

Where the notation  $\tilde{a} = U_C^\dagger a U_C$  is used for the jump operators. If this equation is expanded in the vectorized  $\sigma_x$  basis,  $\tilde{\rho} = \left( \langle + | \tilde{\rho} | + \rangle, \langle + | \tilde{\rho} | - \rangle, \langle - | \tilde{\rho} | + \rangle, \langle - | \tilde{\rho} | - \rangle \right)^T$ ,

$$\frac{d\tilde{\rho}}{dt} = \mathcal{L}_{\text{ind}}(t) \tilde{\rho} \quad (\text{E47})$$

$$\mathcal{L}_{\text{ind}}(t) = \frac{1}{4} \begin{pmatrix} (-\Gamma_\phi - 2\Gamma_1) & \Delta\Gamma_1 e^{-2iG(t)} & \Delta\Gamma_1 e^{2iG(t)} & \Gamma_\phi \\ \Delta\Gamma_1 e^{2iG(t)} & (-8i\xi(t)\lambda(t) - \Gamma_\phi - 2\Gamma_1) & e^{4iG(t)} \Gamma_\phi & \Delta\Gamma_1 e^{2iG(t)} \\ \Delta\Gamma_1 e^{-2iG(t)} & e^{-4iG(t)} \Gamma_\phi & (8i\xi(t)\lambda(t) - \Gamma_\phi - 2\Gamma_1) & \Delta\Gamma_1 e^{-2iG(t)} \\ \Gamma_\phi & \Delta\Gamma_1 e^{-2iG(t)} & \Delta\Gamma_1 e^{2iG(t)} & (-\Gamma_\phi - 2\Gamma_1) \end{pmatrix} \quad (\text{E48})$$

Where  $\Gamma_1 = \Gamma_1^1 + \Gamma_2^1$ ,  $\Delta\Gamma_1 = \Gamma_2^1 - \Gamma_1^1$ , and  $\Gamma_\phi = \Gamma_1^\phi + \Gamma_2^\phi$ . Note that this equation will yield the solution for a single trajectory of  $\xi(t)$ , since  $\xi(t)$  is a random process.

Several simplifications can be made to this equation. First of all, if the driving is periodic, than  $\lambda(t)$  may be replaced with it's average value, as justified previously. The time dependance of  $G(t)$  can be handled in several ways. Depending on the applied control, it may be justified to assume  $g(t)$  is a constant  $g$ , in which case  $G(t) \rightarrow gt$ . This is useful because it would allow for analytical solution of the averaged equations. Here, we have a different physical limit that allows even further simplification. In our experiments,  $g(t)$  is generally on the order of 10MHz, while  $\lambda$ ,  $\gamma$  and  $\Gamma$  are generally less than 1 MHz. Therefore, these quickly rotating terms can be dropped which yields a set of ODEs for  $\tilde{\rho}$  in which the only time dependence in the coefficients comes from  $\xi(t)$ .

Next  $\tilde{\rho}$  must be averaged over  $\xi(t)$ . This can be done using the Shapiro-Loginov equation (as in section E). We can arrive at a set of constant coefficient linear ODEs for the averaged  $\tilde{\rho}$  and  $\mu$  (as defined near Eq. E5),

$$\begin{pmatrix} \dot{\tilde{\rho}} \\ \dot{\mu} \end{pmatrix} = \mathcal{L}_{SL} \begin{pmatrix} \tilde{\rho} \\ \mu \end{pmatrix} \quad (\text{E49})$$

If  $\tilde{\rho}$  is given in the vectorized energy basis,  $\tilde{\rho} = \left( \langle 01 | \tilde{\rho} | 01 \rangle, \langle 01 | \tilde{\rho} | 10 \rangle, \langle 10 | \tilde{\rho} | 01 \rangle, \langle 10 | \tilde{\rho} | 10 \rangle \right)^T$ ,  $\mathcal{L}$  is given by,

$$\mathcal{L}_{SL} = \begin{pmatrix} A & B \\ B & A - \gamma I \end{pmatrix} \quad (\text{E50})$$

$$A = \frac{1}{8} \begin{pmatrix} -4\Gamma_1 - \Gamma_\phi & 0 & 0 & \Gamma_\phi \\ 0 & -4\Gamma_1 - 3\Gamma_\phi & -\Gamma_\phi & 0 \\ 0 & -\Gamma_\phi & -4\Gamma_1 - 3\Gamma_\phi & 0 \\ \Gamma_\phi & 0 & 0 & -4\Gamma_1 - \Gamma_\phi \end{pmatrix} \quad (\text{E51})$$



$$B = i\lambda \begin{pmatrix} 0 & 1 & -1 & 0 \\ 1 & 0 & 0 & -1 \\ -1 & 0 & 0 & 1 \\ 0 & -1 & 1 & 0 \end{pmatrix} \quad (\text{E52})$$

$\mathcal{L}_{SL}$  is analytically diagonalizable, so the dynamics can easily be computed in closed form. Particularly relevant to experiments is the normalized  $\langle \sigma_z \rangle$  observable,

$$\frac{\langle 01 | \tilde{\rho} | 01 \rangle - \langle 10 | \tilde{\rho} | 10 \rangle}{\langle 01 | \tilde{\rho} | 01 \rangle + \langle 10 | \tilde{\rho} | 10 \rangle} = e^{-\frac{1}{4}t(4\gamma + \Gamma_\phi)} \left( \cosh(t\Omega) + \frac{\gamma \sinh(t\Omega)}{\Omega} \right) \quad (\text{E53})$$

$$\Omega = \sqrt{\gamma^2 - 4\lambda^2}$$

Note that this is simply the solution without including white noise (Eq. D8) with an additional exponentially decaying prefactor.

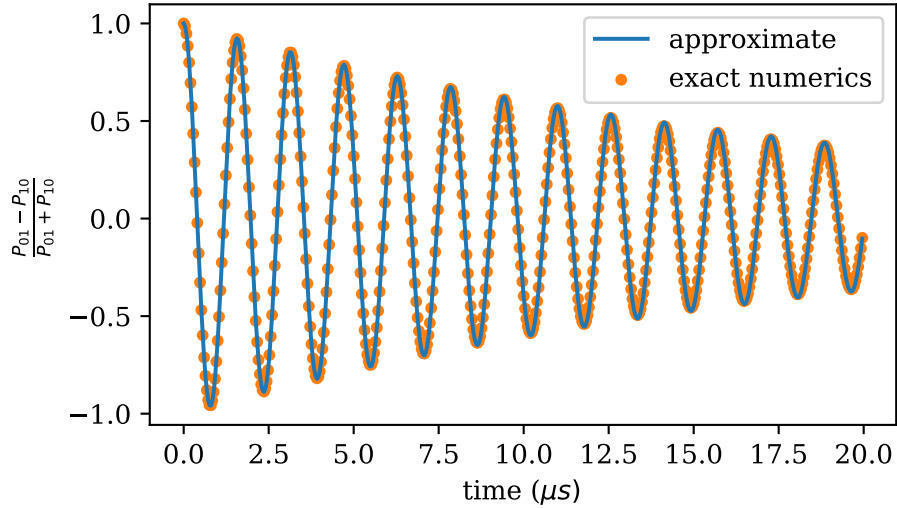


FIG. S1. Comparison of the approximate solution for the decay envelope of the normalized  $\langle \sigma_z \rangle$  in the case of free decay (Eq. E53) to exact numerical simulation of the time dependant master equation constructed using eq. E47.  $g(t)$  was taken to be a 40ns smoothed trapezoidal pulse with a maximum of  $g_{max}$ . Parameter values used here are  $\gamma = 0.05\text{MHz}$ ,  $\lambda = 0.3\text{MHz}$ ,  $g_{max} = 10\text{MHz}$ ,  $\Gamma_\phi = 0.1\text{MHz}$ ,  $\Gamma_1 = 0.15\text{MHz}$ , and  $\Delta\Gamma_1 = 0.05\text{MHz}$ . This represents the strongest noise we ever see experimentally at an artificially lowered  $g$  value, which should be a good stress test the approximation. The approximation seems to work well over a wide range of parameter values. The envelope function oscillates because these parameter values lead to an under-damped solution.

The solution for CPMG pulse sequences can be found using the free decay solution. In line with section D, if the qubit frequency pulses are instantaneous the effective Hamiltonian could be written  $H(t) = h(t)(H_C(t) + H_N(t))$ , where  $h(t)$  is the filter function defined in Eq. D14. In this case, the dynamics for a CPMG sequence of a given length would be given by

$$\begin{pmatrix} \dot{\tilde{\rho}} \\ \dot{\mu} \end{pmatrix} = \dots \mathcal{L}_{\text{even}} \mathcal{L}_{\text{odd}} \mathcal{L}_{\text{odd}} \mathcal{L}_{\text{even}} \begin{pmatrix} \tilde{\rho} \\ \mu \end{pmatrix} \quad (\text{E54})$$

Where  $\mathcal{L}_{\text{even}} = \mathcal{L}(\lambda = \lambda)$  and  $\mathcal{L}_{\text{odd}} = \mathcal{L}(\lambda = -\lambda)$

If we compute the normalized  $\langle \sigma_z \rangle$  observable (as in Eq. D9) using this scheme, we find that it is equivalent to Eq. D26 with a prefactor of  $e^{-\frac{\Gamma_\phi t}{4}}$ .

### Appendix F: Decay Under Gaussian Noise

A bounded integral of a Gaussian random process  $x(t)$  is a Gaussian random variable  $X(t)$ ,

$$X(t) = \int_0^t g(\tau)x(\tau)d\tau \quad (\text{F1})$$

$$\int_0^t |g(\tau)|d\tau < \infty \quad (\text{F2})$$

Therefore, if  $\xi(t)$  is Gaussian noise, decay functions  $\chi(t)$  or  $\chi_{\text{CPMG}}(t)$ , as in Eq. (D16), are given by

$$\chi(t) = \langle e^{2i \int_0^t h(\tau)\xi(\tau)d\tau} \rangle = e^{-\Gamma(t)} \quad (\text{F3})$$

$$\Gamma(t) = 2 \int_0^t d\tau_1 \int_0^t d\tau_2 h(\tau_1)h(\tau_2) \langle \xi(\tau_1)\xi(\tau_2) \rangle \quad (\text{F4})$$

For stationary  $\xi(t)$  the correlator depends only on the time difference,  $\langle \xi(\tau_1)\xi(\tau_2) \rangle = c(\tau_1 - \tau_2)$ , and then  $\Gamma(t)$  can be expressed in terms of the noise power spectrum  $S(\omega) = S(-\omega)$ ,

$$\Gamma(t) = 2 \int_0^\infty \frac{S(\omega)}{\pi} F(\omega, t) d\omega \quad (\text{F5})$$

$$c(\tau_1 - \tau_2) = \int_{-\infty}^\infty \frac{S(\omega)}{2\pi} e^{i\omega(\tau_1 - \tau_2)} d\omega \quad (\text{F6})$$

$$F(\omega, t) = \int_0^t h(\tau_1) e^{i\omega\tau_1} d\tau_1 \int_0^t h(\tau_2) e^{-i\omega\tau_2} d\tau_2 \quad (\text{F7})$$

In the case of Coupler Ramsey measurement  $h(t) = 1$ , and  $F(\omega, t)$  is

$$F(\omega, t) = 4 \frac{\sin^2\left(\frac{\omega t}{2}\right)}{\omega^2} \quad (\text{F8})$$

In the case of 1/f noise  $S(\omega) = \frac{\lambda^2}{\omega}$ , and  $\Gamma(t)$  is

$$\Gamma(t) = - \frac{2\lambda^2 (-1 + \cos(\omega_m t) + \omega_m t (\omega_m t \text{Ci}(\omega_m t) - \sin(\omega_m t)))}{\pi\omega_m^2} \quad (\text{F9})$$

$$\text{Ci}(z) = - \int_z^\infty \frac{\cos(t)}{t} dt \quad (\text{F10})$$

where  $\omega_m$  is the low-frequency cutoff of  $S(\omega)$ . In the experimentally relevant limit where  $\omega_m t$  is small,

$$\Gamma(t) \cong \frac{\lambda^2 t^2}{\pi} (3 - 2\gamma_{\text{Euler}} + 2 \ln\left(\frac{1}{\omega_m t}\right)) \quad (\text{F11})$$

Since  $\ln\left(\frac{1}{\omega_m t}\right)$  is a slowly changing function, Eq. F11 produces approximately Gaussian decay,

$$\chi(t) \cong e^{-\Gamma_G t^2} \quad (\text{F12})$$

$$\Gamma_g \propto \lambda^2 \quad (\text{F13})$$

We can now discuss the case of decay in the presence of CPMG filtering. Let us consider a Gaussian noise with the power spectral density equal to that of a single RTN fluctuator:

$$S(\omega) = \frac{4\lambda^2\gamma}{\omega^2 + 4\gamma^2} \quad (\text{F14})$$

For an arbitrary CPMG sequence with  $n$  echo pulses the decay envelope function is given by the standard expression:

$$\chi(n, T_C) = e^{-\Gamma(n, T_C)}, \quad (\text{F15})$$

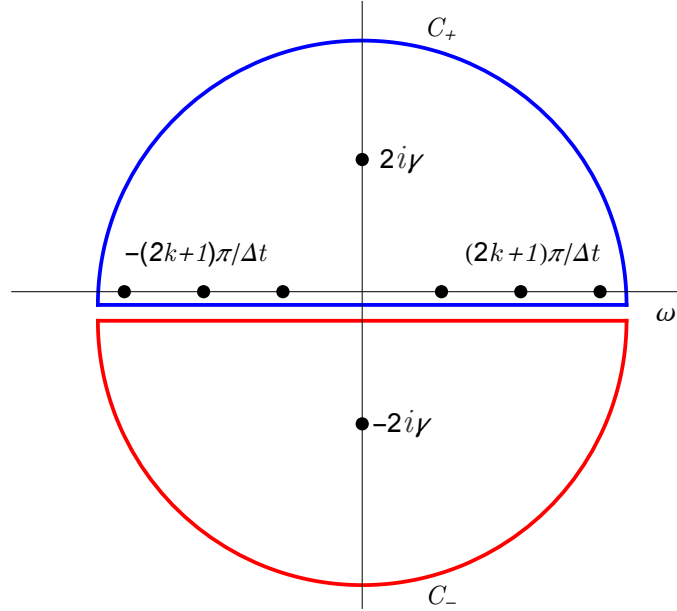


FIG. S2. Integration contours for computing  $\Gamma(n, T_C = \Delta t)$

The filter function in this case is:

$$F(n, \omega T_C) = \frac{1}{\omega^2} \left( 1 - \frac{1}{\cos(\omega T_C/2)} \right)^2 \times \begin{cases} \sin^2(n\omega T_C/2) & \text{if } n \text{ even} \\ \cos^2(n\omega T_C/2) & \text{if } n \text{ odd} \end{cases} \quad (\text{F16})$$

Here  $T_C$  is time interval between two consecutive  $\pi$ -pulses of the  $n$ -pulse sequence such that the total sequence time  $t = nT_C$ . Using Eqs. (F14) and (F16) we can split the integral in Eq. (F5) as follows:

$$\Gamma(n, T_C) = I_0(T_C) - \frac{1}{2}(-1)^n (I_+(n, T_C) + I_-(n, T_C)), \quad (\text{F17})$$

where

$$I_0(T_C) = \frac{1}{2\pi} \int_{-\infty}^{\infty} d\omega \left( \frac{16\lambda^2\gamma}{\omega^2(4\gamma^2 + \omega^2)} + \frac{16\lambda^2\gamma \left( (-1 + \sec(\omega T_C/2))^2 - 1 \right)}{\omega^2(4\gamma^2 + \omega^2)} \right) \quad (\text{F18})$$

$$I_+(n, T_C) = \frac{1}{2\pi} \int_{-\infty}^{\infty} d\omega \frac{16\lambda^2\gamma e^{in\omega T_C} (-1 + \sec(\omega T_C/2))^2}{\omega^2(4\gamma^2 + \omega^2)} \quad (\text{F19})$$

$$I_-(n, T_C) = \frac{1}{2\pi} \int_{-\infty}^{\infty} d\omega \frac{16\lambda^2\gamma e^{-in\omega T_C} (-1 + \sec(\omega T_C/2))^2}{\omega^2(4\gamma^2 + \omega^2)} \quad (\text{F20})$$

The integrands in Eqs. (F18)-(F20) have infinite series of poles at frequencies  $\omega_k = \pm(2k+1)\pi/T_C$  and additional two poles at  $\pm 2i\gamma$  (see Fig S2). To evaluate the integrals  $I_+$  and  $I_-$  we use the contours  $C_+$  and  $C_-$  respectively, as shown in Fig. S2, and obtain:

$$I_+(n, T_C) = \sum_{k=0}^{\infty} \frac{(-1)^{n+1} 32n\lambda^2 T_C}{\pi^2 \gamma (2k+1)^2 (1 + (2k+1)^2 \pi^2 / (2\gamma \Delta t)^2)} - \frac{4\lambda^2 e^{-2n\gamma T_C} \sinh^4(\gamma T_C/2)}{\gamma^2 \cosh^2(\gamma T_C)} \quad (\text{F21})$$

and

$$I_-(n, T_C) = -\frac{4\lambda^2 e^{-2n\gamma T_C} \sinh^4(\gamma T_C/2)}{\gamma^2 \cosh^2(\gamma T_C)} \quad (\text{F22})$$

The integral  $I_0$  can be computed by integrating the first term in Eq. (F18) along the horizontal line proximate to the real axis and lying in the lower half-plane. Then we can close the contour ( $C_-$ ) in the lower half-plane to evaluate the remaining integral along this contour. This yields:

$$I_0(n, T_C) = -\frac{4\lambda^2 \sinh^4(\gamma T_C/2)}{\gamma^2 \cosh^2(\gamma T_C)} \quad (\text{F23})$$

After evaluating the sum in Eq. (F21) and substituting Eqs. (F21)- (F23) into Eq. (F17) we finally obtain:

$$\Gamma(n, T_C) = \frac{2\lambda^2 n}{\gamma^2} (\gamma T_C - \tanh(\gamma T_C)) - \delta\Gamma(n, T_C), \quad (\text{F24})$$

where

$$\delta\Gamma(n, T_C) = \frac{8\lambda^2 e^{-n\gamma T_C} \sinh^4(\gamma T_C/2)}{\gamma^2 \cosh^2(\gamma T_C)} \times \begin{cases} \sinh(n\gamma T_C) & \text{if } n \text{ even} \\ \cosh(n\gamma T_C) & \text{if } n \text{ odd} \end{cases} \quad (\text{F25})$$

Eqs. (F24) and (F25) are exact for any Gaussian noise with a Lorentzian power spectrum and for any  $n$ . They also match the weak-coupling limit of the CPMG formula for a non-Gaussian noise induced by a single random telegraph noise source. For large  $n$  only the first term, proportional to  $n$  is important. This term describes the well-known for the CPMG exponential decay for large  $n$ , with  $\Gamma(n, T_C) \propto n$ .

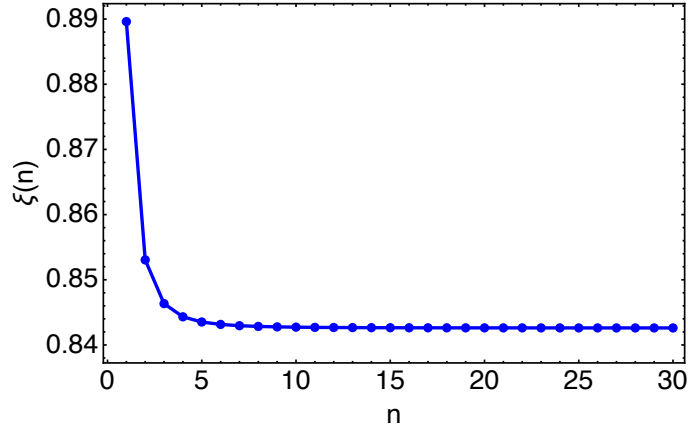


FIG. S3. Dependence of  $\Gamma'(n, T_C)$  on  $n$  for  $1/f$  noise

For  $1/f$ -noise with  $S(\omega) = \frac{\lambda^2}{\omega}$  we find

$$\frac{\partial \Gamma(n, T_C)}{\partial n} = 2T_C^2 \lambda^2 \xi(n) \propto \omega_c^{-2}, \quad (\text{F26})$$

where

$$\xi(n) = \int_0^{\infty} \left( \frac{x - \tanh(x)}{x^3} + \frac{8e^{-2nx} \operatorname{sech}^2(x) \sinh^4\left(\frac{x}{2}\right)}{x^2} \right) dx \quad (\text{F27})$$

only weakly depends on  $n$  (see Fig. S3) and quickly saturates at  $\xi(\infty) = \int_0^\infty (x - \tanh(x)) / x^3 = 0.8525$ . Therefore, letting  $T_C = \frac{t}{n}$

$$\Gamma(t) \cong \frac{2t^2 \lambda^2 \xi(n)}{n} \quad (\text{F28})$$

This describes Gaussian decay with a rate inversely proportional to  $n$ . Therefore, under a Gaussian noise model we would expect that increasing the number of echo pulses that occur in time  $t$  should always increase the amount of noise protection.

### Appendix G: The Smoothness of Decay Under Gaussian Noise

The time derivative of the decay envelope under Gaussian noise is given by,

$$\frac{d\chi(t)}{dt} = -e^{-\Gamma(t)} \frac{d\Gamma(t)}{dt} \quad (\text{G1})$$

The first two terms in this expression are always positive for non-zero  $S(\omega)$ , as  $F(\omega, t)$  is non-negative. Therefore, if zeros are to be present in the derivative of  $\chi(t)$ , the following condition must be met,

$$0 = \frac{d\Gamma(t)}{dt} = \int_0^\infty S(\omega) \frac{dF(\omega, t)}{dt} d\omega \quad (\text{G2})$$

For an even CPMG sequence,  $\frac{dF(\omega, t)}{dt}$  is given by,

$$\frac{dF(\omega, t)}{dt} = \frac{\sin\left(\frac{t\omega}{2}\right) \left(\sec\left(\frac{t\omega}{2n}\right) - 1\right) \left(n \cos\left(\frac{t\omega}{2}\right) \left(\sec\left(\frac{t\omega}{2n}\right) - 1\right) + \sin\left(\frac{t\omega}{2}\right) \tan\left(\frac{t\omega}{2n}\right) \sec\left(\frac{t\omega}{2n}\right)\right)}{n\omega} \quad (\text{G3})$$

Where  $F(\omega, t)$  was obtained by substituting  $T_C = \frac{t}{n}$  into equation F16. Since  $F(\omega, t)$  has the form of a product of  $\omega^{-2}$  and a function of  $\omega t/n$ , the derivative  $dF/dt \propto (\omega n)^{-1}$ . For  $n = 2$ , the function  $dF/dt$  has zeros at,

$$\omega = \frac{8\pi m}{t}, \frac{4\left(\frac{-2\pi}{3} + 2\pi m\right)}{t}, \frac{4\left(\frac{2\pi}{3} + 2\pi m\right)}{t}, m \in \mathbb{Z} \quad (\text{G4})$$

The first positive zero is at  $\omega_0 = \frac{8\pi}{3t_z}$ , and  $F(\omega, t_z) > 0$  for  $\omega < \omega_0$ , as shown in figure S4. It is clear from figure S4 that in order for there to be a single zero in  $\frac{dF(\omega, t)}{dt}$  at  $t = t_z \cong 1500\text{ns}$ , it is necessary that the noise must have much more power at frequencies larger than  $\omega_0 \cong 1\text{MHz}$  than at low frequencies. This requirement directly contradicts modern experimental observations of flux noise in SQUID-based devices [36–39] which find  $1/f$  noise over a range extending well past 1MHz. Additionally, this high frequency power must be concentrated in the regions of frequency where  $\frac{dF(\omega, t)}{dt}$  is positive, which would mean  $S(\omega)$  could not be smooth on the MHz scale. The additional requirements of periodic zeros and non-positivity of the derivative (as seen in the data and predicted by our best non-Gaussian model) make it harder still for a Gaussian model to explain this behavior.

### Appendix H: Fitting to Many CPMG Curves Simultaneously

Figure S5 shows a 2 parameter fit to CPMG curves for 5 different values of  $n$ .

### Appendix I: Echoing Strongly Coupled Fluctuators

Consider a single, far underdamped fluctuator,  $\lambda \gg \gamma$ . Then,

$$\Omega = i\bar{\omega} \quad (\text{I1})$$



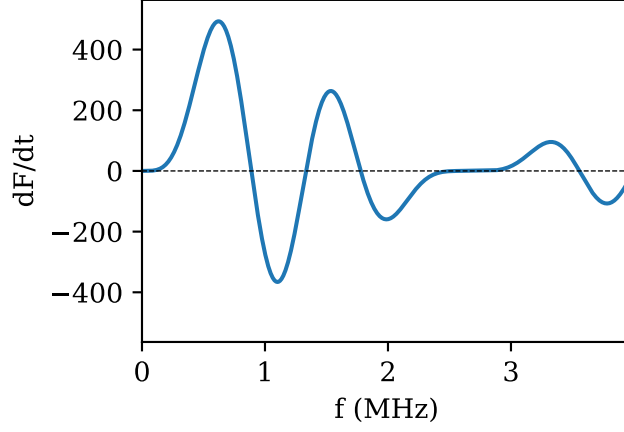


FIG. S4. Plot of  $\frac{dF(\omega,t)}{dt}$  for  $n=2$  and  $t_z = 1500\text{ns}$ ,  $f = \frac{\omega}{2\pi}$ .

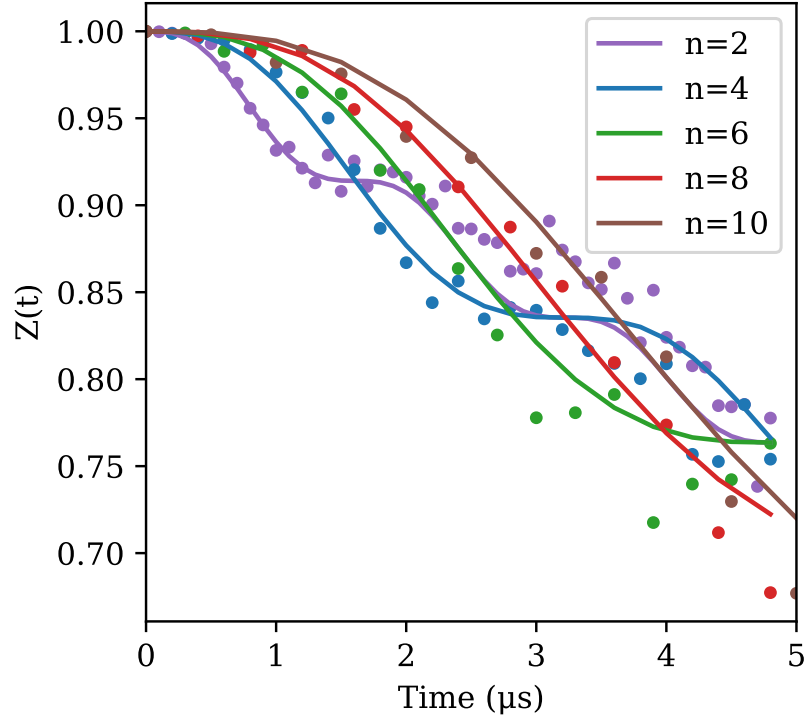


FIG. S5. Fit of the 2 parameter single fluctuator model to 5 CPMG curves simultaneously. As in the main text, the x-axis is real time,  $t = 2mnt_g$ .  $m$  is varied to change the duration of a constant  $n$  CPMG sequence.

Where  $\bar{\omega} = \sqrt{4\lambda^2 - \gamma^2} \approx 2\lambda$  is a real number. If we then make the substitution  $\frac{\gamma}{\bar{\omega}} = \epsilon$ , equation D26 reduces to,

$$\chi(nT_C) \approx e^{-nT_C\gamma} e^{n\epsilon \sin(T_C\bar{\omega})} \quad (\text{I2})$$

If  $n\epsilon \ll 1$ , we can expand to leading order in  $n\epsilon \sin\left(\frac{t\omega}{n}\right)$ ,

$$\chi(nT_C) \approx e^{-nT_C\gamma} (1 + n\epsilon \sin(T_C\bar{\omega})) \quad (\text{I3})$$

The implication of this equation is that for modest  $n$ , increasing the number of echoing pulses will not protect qubits from the dephasing effects of the strongly coupled fluctuator given that we keep  $t = nT_C$  constant. Only when  $n\epsilon > 1$

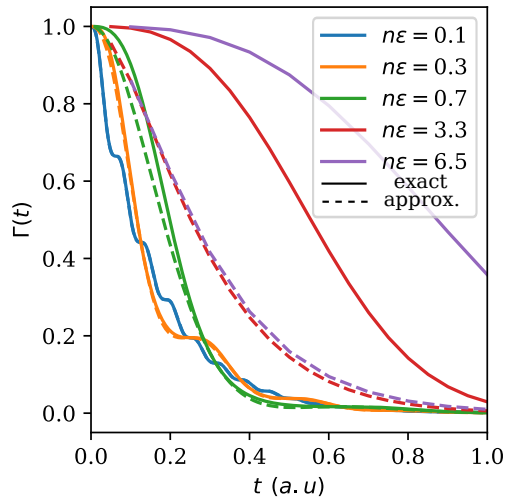


FIG. S6. Comparing exact and analytical solutions for the echoed decay envelope. Exact solutions are calculated using Eq. D26 and are shown in solid lines, while the approximate solutions are calculated using Eq. I3 and are shown by dashed lines. The approximation is almost exact for the two lowest values of  $n\epsilon$ , but has significant error for  $n\epsilon > 1$ .

do we start to see significant protection from the noise. This is shown in figure S6. This behaviour is qualitatively quite different from what happens with gaussian  $1/f$ -type noise, where increasing the number of echo pulses that occur in time  $t$  will move the center of the filter function to higher frequencies and monotonically reduce dephasing.

#### Appendix J: Alternative Explanation of Coupler CPMG

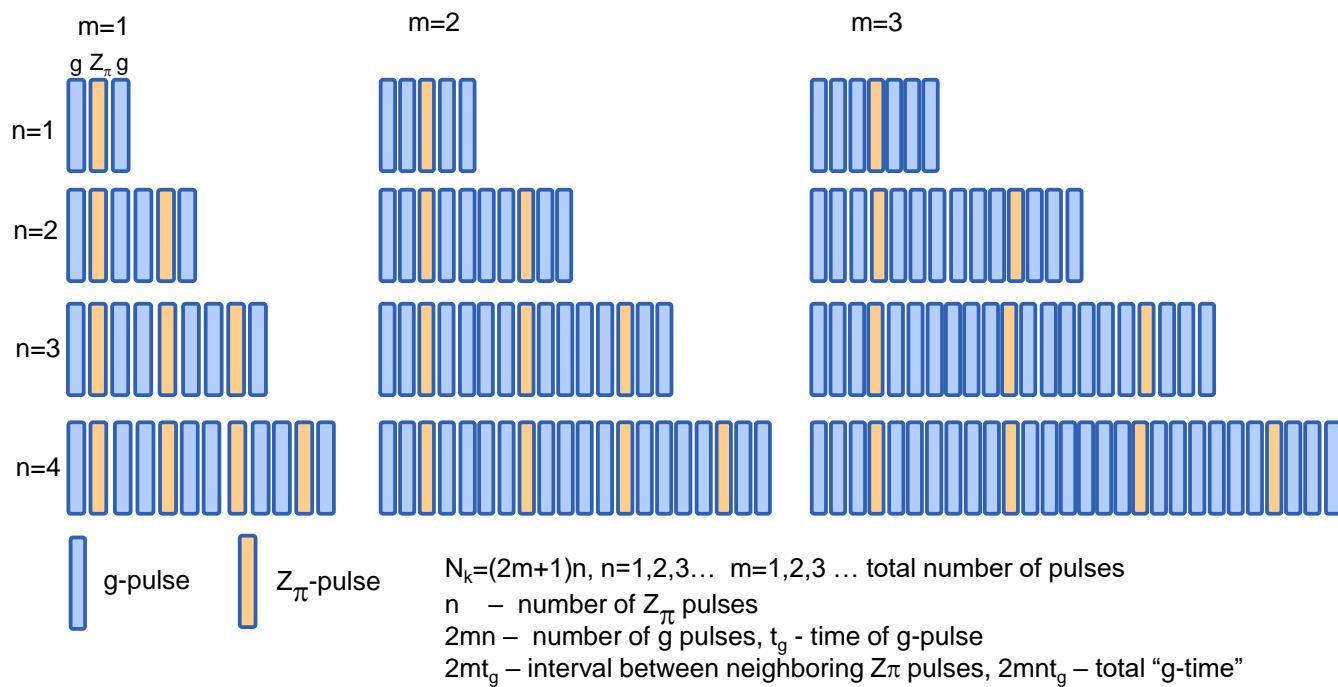


FIG. S7. Examples of the coupler CPMG sequence for different values of  $n$  and  $m$ .